EFFECT OF HEATED WALL POSITION ON MAGNETO-HYDRODYNAMIC MIXED CONVECTION IN A CHANNEL WITH AN OPEN CAVITY

by

Rowshon Ara Begum
Student No. 040809006P
Registration No. 040809006, Session: April-2008

MASTER OF PHILOSOPHY
IN
MATHEMATICS

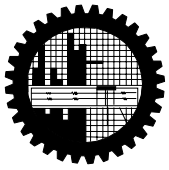

Department of Mathematics
BANGLADESH UNIVERSITY OF ENGINEERING AND TECHNOLOGY, DHAKA-1000
December- 2012

The thesis entitled **"EFFECT OF HEATED WALL POSITION ON MAGNETO-HYDRODYNAMIC MIXED CONVECTION IN A CHANNEL WITH AN OPEN CAVITY",** submitted by **Rowshon Ara Begum**, Roll no: 040809006P, Registration No. 040809006, Session April 2008 has been accepted as satisfactory in partial fulfillment of the requirement for the degree of Master of Philosophy in Mathematics on 15 December 2012.

BOARD OF EXAMINERS

1. _____
Dr. Md. Mustafizur Rahman — Chairman
Professor — (Supervisor)
Department of Mathematics, BUET, Dhaka-1000

2. _____
Head — Member
Department of Mathematics — (Ex-Officio)
BUET, Dhaka-1000

3. _____
Dr. Md. Abdul Maleque — Member
Professor
Department of Mathematics, BUET, Dhaka-1000

4. _____
Dr. Md. Manirul Alam Sarker — Member
Professor
Department of Mathematics, BUET, Dhaka-1000

5. _____
Dr. Md. Tajul Islam — Member
Associate Professor — (External)
Department of Mathematics
Begum Rokeya University, Rangpur

CANDIDATE'S DECLARATION

I am hereby declaring that no portion of the work considered in this thesis has been submitted in support of an application for another degree or qualification of this or any other University or Institute of learning either in home or abroad.

_____

Rowshon Ara Begum

July 2012

CERTIFICATE OF RESEARCH

This is to certify that the work presented in this thesis is carried out by the author under the supervision of Dr. Md. Mustafizur Rahman, Professor, Department of Mathematics, Bangladesh University of Engineering & Technology, Dhaka-1000, Bangladesh.

---------- ----------

Dr. Md. Mustafizur Rahman **Rowshon Ara Begum**

DEDICATED TO MY PARENTS

ACKNOWLEDGEMENT

I would like to express the noteworthy recognizance of Almighty's continual mercy and help without which no work would have been possible to accomplish the goal. I am pleased to acknowledge with gratefulness to my supervisor Dr. Md. Mustafizur Rahman, Professor, Department of Mathematics, Bangladesh University of Engineering and Technology, for his guidance, constant support, intuitive suggestions and relentless encouragement which have been found very benevolent for the outcome of the research.

I would also like to thanks Dr. Md. Manirul Alam Sarker, Professor, Department of Mathematics, Bangladesh University of Engineering and Technology, for his outstanding recommendation and counsel in the course of being successful to reach the objectives of this dissertation. I would also like to express my sincere thanks and gratitude to. Prof Dr. Md. Elias, Head of the Department of Mathematics, BUET, Prof Dr. Md. Mustafa Kamal Chowdhury, Prof. Dr. Md. Abdul Maleque, Prof Dr. Md. Abdul Hakim Khan and Prof. Dr Md Abdul Alim, Department of Mathematics, Bangladesh University of Engineering and Technology, for extending their cordial support and liberal co-operation for performing my M. Phil course.

Finally I express my thanks to all my family members for their supporting me throughout my study in BUET.

ABSTRACT

The effect of heated wall position on magneto- hydrodynamic mixed convection in a channel with an open cavity has been investigated numerically. Magnetic field is acting countering the fluid flow, normal to the vertical wall of the cavity. Three different cases were considered based on heater position in the cavity as the left vertical side (Case 1), bottom side (Case 2) and right vertical side (Case 3). An external flow enters through an opening located at the left side of the channel, passes through the cavity and finally leaves the channel through an exit at the right side. The physical problems are represented mathematically by different sets of governing equations along with the corresponding boundary conditions. Using a class of appropriate transformations, the governing equations along with the boundary conditions are transformed into non-dimensional form, which are then solved by employing a finite-element scheme based on the Galerkin method of weighted residuals. Results are presented in terms of streamlines, isotherms, average Nusselt number along the hot wall, average fluid temperature at the exit port, pressure and temperature gradient in the domain for different combinations of the governing parameters namely Rayleigh number (Ra) at selected values of Hartmann numbers (Ha) and cavity aspect ratio AR. The results indicate that both the flow and the thermal fields strongly depend on the aforesaid parameters. Comparisons with previously published work are performed and the results are found to be in excellent agreement.

TABLE OF CONTENTS

NOMENCLATURE

AR	cavity aspect ratio
B_0	magnetic induction (Wb/m^2)
c_p	specific heat at constant pressure ($J/kg.K$)
g	gravitational acceleration (ms^{-2})
Gr	Grashof number
h	convective heat transfer coefficient ($W/m^2.K$)
H	height of the cavity (m)
Ha	Hartmann number
H_λ	linear shape function
k	thermal conductivity of fluid ($Wm^{-1}K^{-1}$)
L	length of the cavity (m)
n	dimensional distance either along x or y direction (m)
N	non-dimensional distance either along X or Y direction
N_α	quadratic shape function
Nu	Average Nusselt number
p	pressure
P	non-dimensional pressure
Pr	Prandtl number
q_w	heat flux
Ra	Raleigh number
Re	Reynolds number
S_x	surface tractions along X-axis
S_y	surface tractions along Y-axis
T	dimensional fluid temperature (K)
ΔT	dimensional temperature difference (K)
u	velocity in x-direction (m/s)
U	dimensionless horizontal velocity
v	velocity in y-direction (m/s)
V	dimensionless vertical velocity
$\overline{V}$	cavity volume (m^3)
x, y	Cartesian coordinates (m)
X, Y	dimensionless Cartesian coordinates

Greek symbols

α	thermal diffusivity (m^2s^{-1})
β	coefficient of thermal expansion (K^{-1})
θ	dimensionless fluid temperature
$\Delta\theta$	dimensionless temperature difference

μ	dynamic viscosity of the fluid (m^2s^{-1})
v	kinematic viscosity of the fluid (m^2s^{-1})
ρ	density of the fluid (kgm^{-3})
σ	fluid electrical conductivity ($\Omega^{-1}.m^{-1}$)

Subscripts

h	heated wall
i	inlet state

LIST OF TABLES

LIST OF FIGURES

CHAPTER 1

INTRODUCTION

Heat transfer through channel is an important development and an area of very rapid growth in contemporary trend of heat transfer research. The flow of energy carrying fluids through channel is a rapidly growing branch of fluid mechanics and heat transfer. Mixed convection heat transfer in a channel with an open cavity in the presence of magnetic field is a new branch of thermo-fluid mechanics. To describe the heat transport phenomenon, strong background of the hydrodynamics, the convective heat transfer mechanism and the electromagnetic field are prerequisite as they have a symbiotic relationship.

1.1 CONVECTION HEAT TRANSFER

Convective heat transfer is the heat transfer mechanism affected by the flow of fluids. The amount of energy and matter are conveyed by the fluid can be predicted through the convective heat transfer. The convective heat transfer bifurcates into two branches; the natural convection and the forced convection. Forced convection regards the heat transport by induced fluid motion which is forced to happen. This induced flow needs consistent mechanical power. But natural convection differs from the forced convection through the fluid flow driving force which happens naturally. The flows are driven by the buoyancy effect due to the presence of density gradient and gravitational field. The density difference gives rise to buoyancy effects due to which the flow is gyrated. Buoyancy is due to the combined presence of the fluid density gradient and the body force. As the temperature distribution in the natural convection depends on the intensity of the fluid currents which is dependent on the temperature potential itself, the qualitative and quantitative analysis of natural convection heat transfer is very difficult. Numerical investigation instead of theoretical analysis is more needed in this field. Two types of natural convection heat transfer phenomena can be observed in the nature. One is that external free convection that is caused by the heat transfer interaction between a single wall and a very large fluid reservoir adjacent to the wall. Another is that internal free convection which befalls within a channel or cavity.

1.2 MAGNETOHYDRODYNAMICS

Basic phenomenon is that solid or fluid material moving in a magnetic field experiences an electromotive force. If the material is electrically conducting and a current path is available, electric currents ensue. The consequence is that an electromagnetic force due to the interaction of currents and field appears, perturbing the original motion. Therefore, magneto-hydrodynamics (MHD) is the science of the motion of electrically conducting fluids under the influence of applied magnetic forces. The symbiotic interaction between the fluid velocity field and the electromagnetic forces give rise to a flow scenarios; the magnetic field affects the motion. Indeed MHD, like the low frequency electro-technology that developed in the later nineteenth century, is entirely pre-Maxwellian in spirit. Nevertheless MHD is usually regarded as a very contemporary subject. Applications of MHD are electromagnetic pump, the MHD generator using ionized gas as an armature, electromagnetic pumping of liquid metal coolants in nuclear reactors, stirring and levitation (to avoid contamination) in the metallurgical industries, controlled thermonuclear fusion by confining hot ionized deuterium away from all walls by MHD forces led to intensive research on this branch of MHD and the related topic of plasma physics. One of the novelties of MHD is that a gas can have a free surface, not constrained by a rigid wall and prone to waves and instability. A related application is the use of MHD acceleration to shoot plasma into fusion devices or to produce high energy wind tunnels for simulating hypersonic flight. Other potential applications for MHD include electromagnets with fluid conductors, various energy conversion or storage devices, magnetically controlled lubrication by conducting fluids etc.

1.3 APPLICATION

Mixed convection in a channel with an open cavity plays a significant role in many practical applications. Simultaneous convection of buoyancy and forced convection is called as combined or mixed convection, which is of great interest in engineering applications such as nuclear reactors, lakes and reservoirs, cooling process of electronical devices, solar applications, combustion chambers, food processing and float glass production in industry.

1.4 LITERATURE REVIEW

Combined free and forced (mixed) convective flow in which neither the free convection nor the forced convection effects are dominant and both modes are in a comparable level arise in many natural and technological process. Various researchers investigated the effects of mixed convective flows in cavities, channels by using analytical, experimental and numerical methods. Several studies of mixed convection heat transfer in channels with open cavities have been reported in recent years. Leong et al. (2005) performed a numerical study on the mixed convection from an open cavity in a horizontal channel. Authors found that the heat transfer rate was reduced, and the flow became unstable in the mixed convection regime. Papanicolaou and Jaluria (1990, 1992, 1993 and 1994) carried out a series of numerical studies to investigate the combined forced and natural convective cooling of heat dissipating electronic components, located in rectangular enclosure and cooled by an external through flow of air. Moreover, Raji and Hasnaoui (1998a, 1998b) obtained numerical results by using a finite difference procedure for opposing flows mixed (forced and natural) convection flow in a rectangular cavity heated from the side with a constant heat flux and submitted to a laminar cold jet from the bottom of its heated wall. The fluid leaves the cavity via the top or the bottom of the opposite vertical wall. Later on, the same authors i.e. Raji and Hasnaoui (2000) investigated the mixed convection in ventilated cavities where the horizontal top wall and the vertical left wall were prescribed with equal heat fluxes. At the same time, Angirasa (2000) numerically studied and explained the complex interaction between buoyancy and forced flow in a square enclosure with an inlet and a vent situated respectively, at the bottom and top edges of the vertical isothermal surface, where the other three walls are adiabatic. Also, Omri and Nasrallah (1999) performed numerical analysis by a control volume finite element method on mixed convection in a rectangular enclosure with differentially heated vertical sidewalls. Later on, Singh and Sharif (2003) extended their works by considering six placement configurations of the inlet and outlet of a differentially heated rectangular enclosure whereas the previous work was limited to only two different configurations of inlet and outlet. Hsu and Wang (2000) investigated the mixed convective heat transfer where the heat source was embedded on a board mounted vertically on the bottom

wall at the middle in the enclosure. The cooling airflow enters and exits the enclosure through the openings near the top of the vertical sidewalls. Gau et al. (2000) performed experiments on mixed convection in a horizontal rectangular channel with side heating. A numerical study of mixed convection heat transfer in two dimensional open-ended enclosures were investigated by Khanafer et al. (2002) for three different forced flow angle of attack. Wang and Jaluria (2002) numerically investigated the characteristics of the instability and the resulting effect on the heat transfer in mixed convection flow in a horizontal duct with discrete heat sources. A numerical analysis of laminar mixed convection in a channel with an open cavity and a heated wall bounded by a horizontally insulted plate was presented in Manca et al. (2003), where they considered three heating modes: assisting flow, opposing flow and heating from below. Later on, similar problem for the case of assisting forced flow configuration was tested experimentally by Manca et al. (2006). The flow and temperature field for a two-dimensional confined slot jet impinging on an isothermal hot surface computed by Sahoo and Sharif (2004). A finite-volume based computational study of steady laminar forced convection inside a square cavity with inlet and outlet ports was presented in Saeidi and Khodadadi (2006). Recently Rahman et al. (2007) studied numerically the opposing mixed convection in a vented enclosure. They found that with the increase of Reynolds and Richardson numbers the convective heat transfer becomes predominant over the conduction heat transfer and the rate of heat transfer from the heated wall is significantly depended on the position of the inlet port. Aminossadati and Ghasemib (2009) performed a numerical study on the mixed convection in a horizontal channel with a discrete heat source in an open cavity. They considered three different heating modes and found noticeable differences among the indicated three heating modes. Very recently, Oztop (2011) studied the influence of exit opening location on mixed convection in a channel with volumetric heat sources using finite volume method.

Magneto-hydrodynamics (MHD) is that branch of science, which studies the dynamics of electrically conducting fluids in the presence of electromagnetic fields. MHD is usually regarded as a very up to the date subject, because it has many engineering applications such as liquid-metal cooling of nuclear reactors and

electromagnetic casting, etc. MHD studies are mostly focused on convection heat transfer in closed cavities. Piazza and Ciofalo (2002) carried out a numerical investigation on buoyancy-driven magneto-hydrodynamic flow in a liquid-metal filled in a cubic enclosure. The authors found that increasing Hartmann number suppressed the convective motions. Chamkha (2002) made a study for mixed convection in a square cavity in the presence of magnetic field and an internal heat generation and absorption. He concluded that the flow behavior inside the cavity and heat transfer rate is strongly affected by the magnetic field. Mahmud et al. (2003) studied analytically a combined free and forced convection flow of an electrically conducting and heat-generating/ absorbing fluid a vertical channel made of two parallel plates under the action of transverse magnetic field. Sarries et al. (2005) performed a numerical study on unsteady natural convection of an electrically conducting fluid in a laterally and volumetrically heated square cavity under the influence of a magnetic field. Xu et al. (2006) completed an experimental study on natural convection of a molten metal contained in a rectangular enclosure in the presence of an external magnetic field. Sposito and Ciofalo (2008) studied fully developed mixed magnetohydrodynamic convection in a vertical square duct. Oztop et al. (2009) studied the effects of sinusoidal temperature boundary conditions on magnetohydrodynamic buoyancy-induced flow in a non-isothermally heated square enclosure. Ogot (2010) made an analysis of heat and fluid flow transport due to natural convection and magnetohydrodynamic flows in a square enclosure with a finite length heater using differential quadrature technique. Rahman et al. (2011a) worked on a conjugated effect of joule heating and magnetohydrodynamic on double-diffusive mixed convection in a horizontal channel with an open cavity. Rahman et al. (2011b) examined the magnetohydrodynamic mixed convection in a horizontal channel with an open cavity with Galerkin weighted residual method for the numerical simulation. They showed a significant effect of the considered parameters on the flow and thermal fields inside the cavity. Bhuvaneswari et al. (2011) carried out a computational study of convective flow and heat transfer in a cavity in the presence of uniform magnetic field.

1.5 MOTIVATION

Leong et al. (2005) performed a numerical study on the mixed convection from an open cavity in a horizontal channel. The effects of discrete heat source in an open cavity with a horizontal channel by using control volume method Aminossadati and Ghasemib (2009) has been studied numerically. From the literature review it is clear that very little numerical study on the effect of mixed convection heat transfer in a channel with an open cavity. Thus far, none have conducted studies involving the effect of heated wall position on magneto- hydrodynamic mixed convection in a channel with an open cavity, although it has numerous engineering applications. Numerical studies are therefore essential to observe the variation in fluid flow and heat transfer due to the above physical changes, which forms the basis of the motivation behind the present study. Contextually the present study will focus on the computational analysis of the influence of magnetic field on the mixed convection in a channel with an open cavity.

1.6 OBJECTIVES

The investigation is carried out in a two dimensional horizontal channel with an open cavity. In case 1, case 2 and case 3, left side, bottom side and right side are heated under constant temperature respectively. Remaining solid walls are adiabatic. The specific objectives of the present research work are as follows:

- To develop a mathematical model for mixed convection in a channel with an open cavity considering magnetic effect and hence to solve that model using finite element method.
- To carry out the validation of the present finite element model by investigating the effect of laminar mixed convection in a channel with an open cavity.
- To investigate the effects of heater location in an open cavity for different Rayleigh number.
- To investigate the effect of Hartmann number, cavity aspect ratio and Rayleigh number on the flow and thermal fields.
- To investigate the effect of Hartmann number, cavity aspect ratio and Rayleigh number on the average Nusselt number, average fluid temperature at the exit port, pressure and temperature gradient in the domain.

1.7 OUTLINE OF THE THESIS

This dissertation contains four chapters. In this chapter a brief introduction is presented with aim and objective. There is nothing new to say about it. This chapter also consists a literature review of the past studies on fluid flow and heat transfer in cavities or channels. In this state-of-the art review, different aspects of the previous studies have been mentioned categorically. This is followed by the post-mortem of a recent historical event for the illustration of fluid flow and heat transfer effects in cavities or channels.

Chapter 2 presents mathematical model along with the computational procedure of the problem.

In Chapter 3 a detailed results and discussion is conducted.

Finally, in Chapter 4 the dissertation is rounded of with the conclusions and recommendations for further study of the present problem are outlined.

CHAPTER 2

MATHEMATICAL MODELLING

Mathematical model of physical phenomena may be ordinary or partial differential equations, which have been the subject of analytical and numerical investigations. The partial differential equations of fluid mechanics and heat transfer are solvable for only a limited number of flows. To obtain an approximate solution numerically, we have to use a discretization method, which approximated the differential equations by a system of algebraic equations, which can then be solved on a computer. The approximations are applied to small domains in space and /or time so the numerical solution provides results at discrete locations in space and time. Much as the accuracy of experimental data depends on the quality of the tools used, the accuracy of numerical solutions depend on the quality of discretizations used. Computational fluid dynamics (CFD) computation involves the formation of a set numbers that constitutes a practical approximation of a real life system. The outcome of computation process improves the understanding of the performance of a system. Thereby, engineers need CFD codes that can make physically realistic results with good quality accuracy in simulations with finite grids. Contained within the broad field of computational fluid dynamics are activities that cover the range from the automation of well established engineering design methods to the use of detailed solutions of the Navier-Stokes equations as substitutes for experimental research into the nature of complex flows. CFD have been used for solving wide range of fluid dynamics problem. It is more frequently used in fields of engineering where the geometry is complicated or some important feature that cannot be dealt with standard methods.

The remainder of this chapter is as follows. In section 2.1, the physical configurations of the current research interest are shown. Then the appropriate mathematical model (both governing equations and boundary conditions) is considered in section 2.2. After that a numerical scheme that is employed in this study are described in the section 2.3.

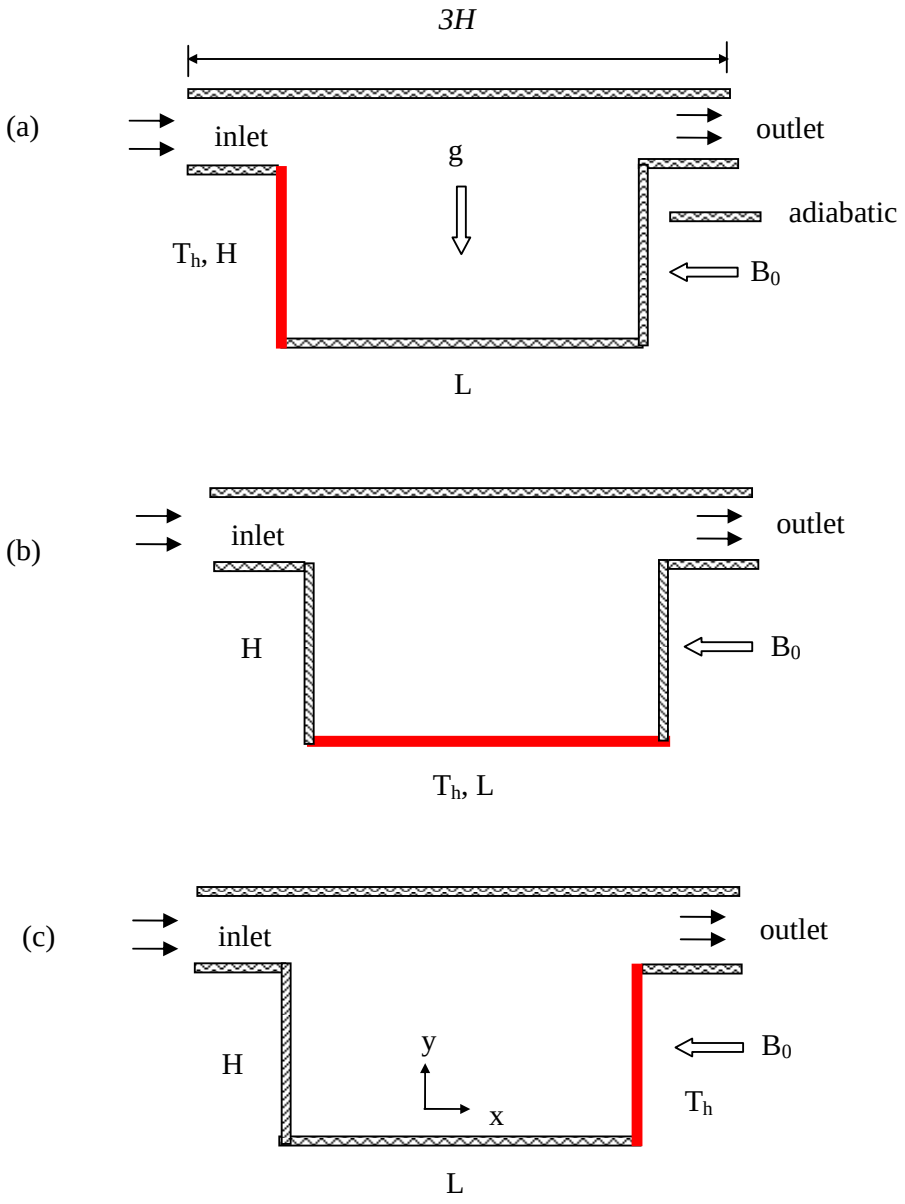

Fig. 2.1. Physical model under consideration: (a) heating from left, (b) heating from below, and (c) heating from right.

2.1 PHYSICAL MODEL

Considered model is presented in Fig. 1 (a) to (c). In these figures, channel includes a square cavity and magnetic field affects in –x direction and gravity acts in the vertical direction. Flow inlets to channel via inlet port at a uniform velocity, u_i, temperature, T_i and exits the channel via outlet port. The length of channel is chosen as 3H, length and height of the cavity are defined by L and H respectively. In case 1, case 2 and case 3, left side, bottom side and right side are heated under constant temperature, T_h respectively. Remaining solid walls are adiabatic.

2.2 GOVERNING EQUATIONS ALONG WITH BOUNDARY CONDITIONS

The electrically conducting fluids are assumed to be Newtonian fluids with constant fluid properties, except for the density in the buoyancy force term. Moreover, the fluid is considered to be laminar, incompressible, steady and two-dimensional. The electrically conducting fluids interact with an external horizontal uniform magnetic field of constant magnetic flux density B_0. Assuming that the flow-induced magnetic field is very small compared to B_0 and considering electrically insulated cavity walls. The electromagnetic force can be reduced to the damping factor $-B_0\upsilon$ (Rahman et al (2009)), where v is the vertical velocity component. Thus the Lorentz force depends only on the velocity component perpendicular to the magnetic field. The governing equations for the two-dimensional steady flow after invoking the Boussinesq approximation and neglecting radiation and viscous dissipation can be expressed as

Continuity Equation

$$\frac{\partial u}{\partial x}+\frac{\partial v}{\partial y}=0 \tag{2.1}$$

Momentum Equations

$$u\frac{\partial u}{\partial x}+v\frac{\partial u}{\partial y}=-\frac{1}{\rho}\frac{\partial p}{\partial x}+\upsilon\left(\frac{\partial^2 u}{\partial x^2}+\frac{\partial^2 u}{\partial y^2}\right) \tag{2.2}$$

$$u\frac{\partial v}{\partial x}+v\frac{\partial v}{\partial y}=-\frac{1}{\rho}\frac{\partial p}{\partial y}+\upsilon\left(\frac{\partial^2 v}{\partial x^2}+\frac{\partial^2 v}{\partial y^2}\right)+g\beta\left(T-T_i\right)-\frac{\sigma {B_0}^2 v}{\rho} \tag{2.3}$$

Energy Equations

$$u\frac{\partial T}{\partial x}+v\frac{\partial T}{\partial y}=\frac{k}{\rho c_p}\left(\frac{\partial^2 T}{\partial x^2}+\frac{\partial^2 T}{\partial y^2}\right) \tag{2.4}$$

where x and y are the distances measured along the horizontal and vertical directions respectively; u and v are the velocity components in the x and y directions respectively; T denote the fluid temperature, T_i denotes the reference temperature for which buoyant force vanishes, p is the pressure and ρ is the fluid density, g is the gravitational constant, β is the volumetric coefficient of thermal expansion, c_p is the fluid specific heat, k is the thermal conductivity of fluid.

2.2.1 Boundary Conditions

The boundary conditions for the present problem are specified as follows:

At the inlet: $u=u_i, v=0,\ T=T_i$

At the outlet: $\frac{\partial u}{\partial x}=0, v=0, \frac{\partial T}{\partial x}=0$

at all solid boundaries other than heated wall: $u=v=\frac{\partial T}{\partial n}=0$

At the heated wall: $u=v=0, T=T_h$

where n is the non-dimensional distances either along x or y direction acting normal to the surface and k is the thermal conductivity of the fluid.

Such local values have been further averaged over the entire heated surface to obtain the surface averaged or overall mean Nusselt number

$$Nu=-\frac{1}{L_s}\int_0^{L_s}\frac{\partial T}{\partial N}ds$$

where L_s is the length of the heated wall. The average Nusselt number can be used in process engineering design calculations to estimate the rate transfer from the heated surface.

2.2.2 Dimensional Analysis

Non-dimensional variables are used for making the governing equations (2.1−2.4) into dimensionless form are stated as follows:

$$X = \frac{x}{H},\ Y = \frac{y}{H},\ U = \frac{u}{u_i},\ V = \frac{v}{u_i},\ P = \frac{\left(p + \rho g y\right) H^2}{\rho {u_i}^2},\ \theta = \frac{\left(T - T_i\right)}{\left(T_h - T_i\right)}$$

where X and Y are the coordinates varying along horizontal and vertical directions, respectively, U and V are the velocity components in the X and Y directions, respectively, θ is the dimensionless temperature and P is the dimensionless pressure. After substitution the dimensionless variables into the equations (2.1-2.4), we get the following dimensionless equations as

Continuity Equation

$$\frac{\partial U}{\partial X} + \frac{\partial V}{\partial Y} = 0 \tag{2.5}$$

Momentum Equations

$$U\frac{\partial U}{\partial X} + V\frac{\partial U}{\partial Y} = -\frac{\partial P}{\partial X} + \frac{1}{Re}\left(\frac{\partial^2 U}{\partial X^2} + \frac{\partial^2 U}{\partial Y^2}\right) \tag{2.6}$$

$$U\frac{\partial V}{\partial X} + V\frac{\partial V}{\partial Y} = -\frac{\partial P}{\partial Y} + \frac{1}{Re}\left(\frac{\partial^2 V}{\partial X^2} + \frac{\partial^2 V}{\partial Y^2}\right) + \frac{Ra}{Re^2\, Pr}\theta - \frac{Ha^2}{Re}V \tag{2.7}$$

Energy Equations

$$U\frac{\partial \theta}{\partial X} + V\frac{\partial \theta}{\partial Y} = \frac{1}{Re\, Pr}\left(\frac{\partial^2 \theta}{\partial X^2} + \frac{\partial^2 \theta}{\partial Y^2}\right) \tag{2.8}$$

The dimensionless parameters appearing in the equations (2.6) through (2.8) are the Reynolds number *Re*, Prandtl number *Pr*, Rayleigh number *Ra*, and Hartmann number Ha. They are respectively defined as follows:

$$Re = \frac{UH}{\upsilon},\ Pr = \frac{\upsilon}{\alpha},\ Ra = \frac{g\beta\Delta T H^3}{\nu\alpha},\ Ha^2 = \frac{\sigma B_0^2 H^2}{\mu}$$

where $\Delta T = T_h - T_i \; and \; \alpha = k/\rho C_p$ are the temperature difference and thermal diffusivity of the fluid respectively.

The dimensionless boundary conditions under consideration can be written as:

At the inlet: $U = 1,\ V = 0,\ \theta = 0$

At the outlet: $\frac{\partial U}{\partial X} = 0, V = 0, \frac{\partial \theta}{\partial X} = 0$

at all solid boundaries other than heated wall: $U = 0, V = 0, \frac{\partial \theta}{\partial N} = 0$

at the heated wall: $U = V = 0,\ \theta = 1$

where N is the non-dimensional distances either along X or Y direction acting normal to the surface. According to Singh and Sharif (2003), the average Nusselt number at the heated wall of the cavity based on the no-dimensional variables may be expressed as $Nu = -\int_0^{L_h/L} \frac{\partial \theta}{\partial N} dS$.

where L_h is the length of the heated wall and N is the non-dimensional distances either X or Y direction acting normal to the surface.

2.3 NUMERICAL ANALYSIS

The governing equations along with the boundary conditions are solved numerically, employing Galerkin weighted residual finite element techniques discussed below.

2.3.1 Finite Element Formulation and Computational Procedure

To derive the finite element equations, the method of weighted residuals Zienkiewicz and Taylor (1991) is applied to the equations (2.5) – (2.8) as

$$\int_A N_\alpha \left(\frac{\partial U}{\partial X} + \frac{\partial V}{\partial Y} \right) dA = 0 \qquad (2.9)$$

$$\int_A N_\alpha \left(U \frac{\partial U}{\partial X} + V \frac{\partial U}{\partial Y} \right) dA = -\int_A H_\lambda \left(\frac{\partial P}{\partial X} \right) dA + \frac{1}{Re} \int_A N_\alpha \left(\frac{\partial^2 U}{\partial X^2} + \frac{\partial^2 U}{\partial Y^2} \right) dA \qquad (2.10)$$

$$\int_A N_\alpha \left(U\frac{\partial V}{\partial X} + V\frac{\partial V}{\partial Y} \right) dA = -\int_A H_\lambda \left(\frac{\partial P}{\partial Y} \right) dA + \frac{1}{Re}\int_A N_\alpha \left(\frac{\partial^2 V}{\partial X^2} + \frac{\partial^2 V}{\partial Y^2} \right) dA + \frac{Ra}{Re^2 Pr}\int_A N_\alpha \theta \, dA - \frac{Ha}{Re}\int_A N_\alpha V \, dA \tag{2.11}$$

$$\int_A N_\alpha \left(U\frac{\partial \theta}{\partial X} + V\frac{\partial \theta}{\partial Y} \right) dA = \frac{1}{Re\,Pr}\int_A N_\alpha \left(\frac{\partial^2 \theta}{\partial X^2} + \frac{\partial^2 \theta}{\partial Y^2} \right) dA \tag{2.12}$$

where A is the element area, N_α (α = 1, 2, … … , 6) are the element interpolation functions for the velocity components and the temperature, and H_λ (λ = 1, 2, 3) are the element interpolation functions for the pressure.

Gauss's theorem is then applied to equations (2.10)-(2.12) to generate the boundary integral terms associated with the surface tractions and heat flux. Then equations (2.10)-(2.12) become,

$$\int_A N_\alpha \left(U\frac{\partial U}{\partial X} + V\frac{\partial U}{\partial Y} \right) dA + \int_A H_\lambda \left(\frac{\partial P}{\partial X} \right) dA + \frac{1}{Re}\int_A \left(\frac{\partial N_\alpha}{\partial X}\frac{\partial U}{\partial X} + \frac{\partial N_\alpha}{\partial Y}\frac{\partial U}{\partial Y} \right) dA = \int_{S_0} N_\alpha S_x dS_0 \tag{2.13}$$

$$\int_A N_\alpha \left(U\frac{\partial V}{\partial X} + V\frac{\partial V}{\partial Y} \right) dA + \int_A H_\lambda \left(\frac{\partial P}{\partial Y} \right) dA + \frac{1}{Re}\int_A \left(\frac{\partial N_\alpha}{\partial X}\frac{\partial V}{\partial X} + \frac{\partial N_\alpha}{\partial Y}\frac{\partial V}{\partial Y} \right) dA - \frac{Ra}{Re^2 Pr}\int_A N_\alpha \, \theta \, dA + \frac{Ha^2}{Re}\int_A N_\alpha V \, dA = \int_{S_0} N_\alpha S_y dS_0 \tag{2.14}$$

$$\int_A N_\alpha \left(U\frac{\partial \theta}{\partial X} + V\frac{\partial \theta}{\partial Y} \right) dA + \frac{1}{Re.Pr}\int_A \left(\frac{\partial N_\alpha}{\partial X}\frac{\partial \theta}{\partial X} + \frac{\partial N_\alpha}{\partial Y}\frac{\partial \theta}{\partial Y} \right) dA = \int_{S_w} N_\alpha \, q_w \, dS_w \tag{2.15}$$

Here (2.13)-(2.14) specifying surface tractions (S_x, S_y) along outflow boundary S_0 and (2.15) specifying velocity components and fluid temperature or heat flux (q_w) that flows into or out from domain along wall boundary S_w.

The basic unknowns for the above differential equations are the velocity components U, V the temperature, θ and the pressure, P. The six node triangular element is used in this work for the development of the finite element equations. All six nodes are associated with velocities as well as temperature; only the corner nodes are associated with pressure. This means that a lower order polynomial is chosen for

pressure and which is satisfied through continuity equation. The velocity component and the temperature distributions and linear interpolation for the pressure distribution according to their highest derivative orders in the differential equations (2.5)-(2.8) as

$$U(X,Y) = N_\beta U_\beta \tag{2.16}$$

$$V(X,Y) = N_\beta V_\beta \tag{2.17}$$

$$\theta(X,Y) = N_\beta \theta_\beta \tag{2.18}$$

$$P(X,Y) = H_\lambda P_\lambda \tag{2.19}$$

where β = 1, 2, … … , 6; λ = 1, 2, 3.

Substituting the element velocity component distributions, the temperature distribution, and the pressure distribution from equations (2.16)-(2.19), the finite element equations can be written in the form,

$$K_{\alpha\beta^x} U_\beta + K_{\alpha\beta^y} V_\beta = 0 \tag{2.20}$$

$$K_{\alpha\beta\gamma^x} U_\beta U_\gamma + K_{\alpha\beta\gamma^y} V_\gamma U_\gamma + M_{\alpha\mu^x} P_\mu + \frac{1}{Re}\left(S_{\alpha\beta^{xx}} + S_{\alpha\beta^{yy}}\right) U_\beta = Q_{\alpha^u} \tag{2.21}$$

$$\begin{aligned} &K_{\alpha\beta\gamma^x} U_\beta V_\gamma + K_{\alpha\beta\gamma^y} V_\beta V_\gamma + M_{\alpha\mu^y} P_\mu + \frac{1}{Re}\left(S_{\alpha\beta^{xx}} + S_{\alpha\beta^{yy}}\right) V_\beta \\ &- \frac{Ra}{Re^2\, Pr} K_{\alpha\beta}\theta_\beta + \frac{Ha^2}{Re} K_{\alpha\beta} V_\beta = Q_{\alpha^v} \end{aligned} \tag{2.22}$$

$$K_{\alpha\beta\gamma^x} U_\beta \theta_\gamma + K_{\alpha\beta\gamma^y} V_\beta \theta_\gamma + \frac{1}{Re.Pr}\left(S_{\alpha\beta^{xx}} + S_{\alpha\beta^{yy}}\right)\theta_\beta = Q_{\alpha\theta} \tag{2.23}$$

where the coefficients in element matrices are in the form of the integrals over the element area and along the element edges S_0 and S_w as

$$K_{\alpha\beta^x} = \int_A N_\alpha N_{\beta,x} dA \tag{2.24a}$$

$$K_{\alpha\beta^y} = \int_A N_\alpha N_{\beta,y} dA \tag{2.24b}$$

$$K_{\alpha\beta\gamma^x} = \int_A N_\alpha N_\beta N_{\gamma,x} dA \tag{2.24c}$$

$$K_{\alpha\beta\gamma^y} = \int_A N_\alpha N_\beta N_{\gamma,y} dA \tag{2.24d}$$

$$K_{\alpha\beta} = \int_A N_\alpha N_\beta dA \tag{2.24e}$$

$$S_{\alpha\beta^{xx}} = \int_A N_{\alpha,x} N_{\beta,x} dA \tag{2.24f}$$

$$S_{\alpha\beta^{yy}} = \int_A N_{\alpha,y} N_{\beta,y} dA \tag{2.24g}$$

$$M_{\alpha\mu^x} = \int_A H_\alpha H_{\mu,x} dA \tag{2.24h}$$

$$M_{\alpha\mu^y} = \int_A H_\alpha H_{\mu,y} dA \tag{2.24i}$$

$$Q_{\alpha^u} = \int_{S_0} N_\alpha S_x dS_0 \tag{2.24j}$$

$$Q_{\alpha^v} = \int_{S_0} N_\alpha S_y dS_0 \tag{2.24k}$$

$$Q_{\alpha^\theta} = \int_{S_w} N_\alpha \, q_w dS_w \tag{2.24l}$$

These element matrices are evaluated in closed form ready for numerical simulation. Details of the derivation for these element matrices are omitted herein.

The derived finite element equations (2.20)-(2.23) are nonlinear. These nonlinear algebraic equations are solved by applying the Newton-Raphson iteration technique by first writing the unbalanced values from the set of the finite element equations (2.20)-(2.23) as,

$$F_{\alpha^p} = K_{\alpha\beta^x} U_\beta + K_{\alpha\beta^y} V_\beta \tag{2.25a}$$

$$\begin{aligned} F_{\alpha^u} &= K_{\alpha\beta\gamma^x} U_\beta U_\gamma + K_{\alpha\beta\gamma^y} V_\gamma U_\gamma + M_{\alpha\mu^x} P_\mu \\ &\quad + \frac{1}{Re}(S_{\alpha\beta^{xx}} + S_{\alpha\beta^{yy}}) U_\beta - Q_{\alpha^u} \end{aligned} \tag{2.25b}$$

$$\begin{aligned} F_{\alpha^v} &= K_{\alpha\beta\gamma^x} U_\beta V_\gamma + K_{\alpha\beta\gamma^y} V_\gamma V_\gamma + M_{\alpha\mu^y} P_\mu + \\ &\quad \frac{1}{Re}(S_{\alpha\beta^{xx}} + S_{\alpha\beta^{yy}}) V_\beta - Ri\, K_{\alpha\beta}\theta_\beta - Q_{\alpha^v} \end{aligned} \tag{2.25c}$$

$$F_{\alpha^\theta} = K_{\alpha\beta\gamma^x} U_\beta \theta_\gamma + K_{\alpha\beta\gamma^y} V_\beta \theta_\gamma + \frac{1}{Re.Pr}\left(S_{\alpha\beta^{xx}} + S_{\alpha\beta^{yy}}\right)\theta_\beta - Q_{\alpha^\theta} \tag{2.25d}$$

This leads to a set of algebraic equations with the incremental unknowns of the element nodal velocity components, temperatures, and pressures in the form,

$$\begin{bmatrix} K_{pu} & K_{pv} & 0 & 0 \\ K_{uu} & K_{uv} & 0 & K_{up} \\ K_{\theta u} & K_{\theta v} & K_{\theta\theta} & 0 \\ K_{vu} & K_{vv} & K_{v\theta} & K_{vp} \end{bmatrix} \begin{Bmatrix} \Delta p \\ \Delta u \\ \Delta \theta \\ \Delta v \end{Bmatrix} = - \begin{Bmatrix} F_{\alpha^p} \\ F_{\alpha^u} \\ F_{\alpha^\theta} \\ F_{\alpha^v} \end{Bmatrix} \tag{2.26}$$

where $K_{uu} = K_{\alpha\beta\gamma^x} U_\beta + K_{\alpha\gamma\beta^x} U_\gamma + K_{\alpha\beta\gamma^y} V_\beta + \frac{1}{Re}\left(S_{\alpha\beta^{xx}} + S_{\alpha\beta^{yy}} \right)$

$K_{uv} = K_{\alpha\beta\gamma^y} U\gamma$

$K_{u\theta} = 0,\ K_{up} = M_{\alpha\mu^x}$

$K_{vu} = K_{\alpha\beta\gamma^x} V\gamma$

$K_{vv} = K_{\alpha\beta\gamma^x} U_\beta + K_{\alpha\gamma\beta^y} V_\gamma + K_{\alpha\beta\gamma^y} V_\gamma + \frac{1}{Re}\left(S_{\alpha\beta^{xx}} + S_{\alpha\beta^{yy}} \right)$

$K_{v\theta} = -Ri\, K_{\alpha\beta},\ K_{vp} = M_{\alpha\mu^y}$

$K_{\theta u} = K_{\alpha\beta\gamma^x} \theta\gamma,\ K_{\theta v} = K_{\alpha\beta\gamma^y} \theta\gamma$

$K_{\theta\theta} = K_{\alpha\beta\gamma^x} U_\beta + K_{\alpha\beta\gamma^y} V_\beta + \frac{1}{Re.Pr}(S_{\alpha\beta^{xx}} + S_{\alpha\beta^{yy}})$

$K_{\theta p} = 0,\ K_{pu} = K_{\alpha\beta^x},\ K_{pv} = K_{\alpha\beta^y}$ and $K_{p\theta} = K_{pp} = 0$

The iteration process is terminated if the percentage of the overall change compared to the previous iteration is less than the specified value.

To solve the sets of the global nonlinear algebraic equations in the form of matrix, the Newton-Raphson iteration technique has been adapted through PDE solver with MATLAB interface. The convergence of solutions is assumed when the relative error for each variable between consecutive iterations is recorded below the convergence

criterion ε such that $\left|\Psi^{n+1} - \Psi^{n}\right| < \varepsilon$, where n is number of iteration and $\Psi = U, V, \theta$. The convergence criterion was set to $\varepsilon = 10^{-5}$.

2.3.2 Grid Size Sensitivity Test

The grid sensitivity tests are performed to locate the field variables grid-independence solutions. Non-uniform triangular element grid system is employed in the present study. Five different non-uniform grid systems with the following number of elements within the resolution field: 3536, 5120, 6248 8106 and 9636 are examined. The numerical simulation is carried out for a highly accurate solution in the average Nusselt number for the aforesaid elements to develop an understanding of the grid fineness as shown in Fig. 2.2. The magnitudes of the average number for 5120 elements show a very little difference with the results obtained for the other elements. Thus the grid independence tests showed that a grid of 5120 elements is enough for the desired accuracy of results.

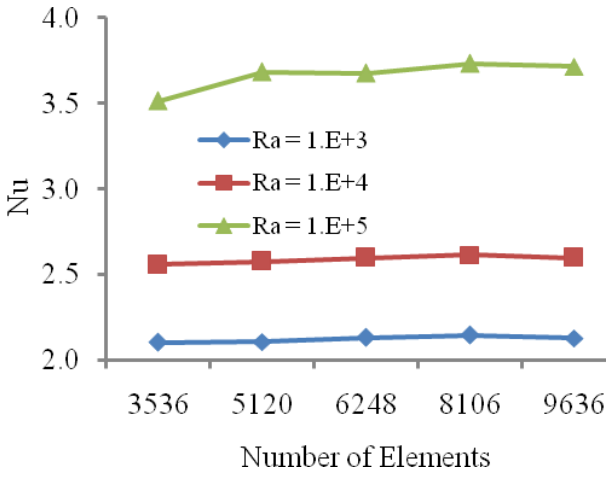

Fig. 2.2. Grid independency study: average Nusselt number at different grid elements for case1 and Ha = 10

2.3.3 Validation of the Numerical Scheme

Due to lack of suitable experimental results in the literature pertaining to the present configuration, the obtained numerical result has been validated against the existing numerical result for channel with an open cavity. For this reason, the present numerical model is validated against the numerical results of Manca et al. (2003) for mixed convection problem in a channel with an open cavity. The calculated average Nusselt number and maximum fluid temperature for the test case are shown in Table 1. The agreement between the present computation and those of Manca et al. (2003) are seen to be very well with a maximum difference within 0.5%. These validations make a good confidence in the present numerical code.

Table 2.1. Comparison of results for validation at Pr = 0.71, Re = 100, Ri = 0.1, w/H = 0.5, L/H = 2

Opposing flow	Present	Manca et al. (2003)
Nu	1.7657	1.7748
θ_{max}	0.629	0.627

CHAPTER 3

RESULTS AND DISCUSSION

As stated earlier, the overall objective of the current chapter is to explore the conjugate effects of conduction and laminar mixed convection heat transfer in an open channel with a rectangular cavity in the presence of a magnetic field. A numerical investigation has been performed in this work for different temperature conditions at different Rayleigh numbers in the enclosure. Three different cases were tested according to heated part of the enclosure. In the first case, heater is located on the left vertical wall of the enclosure, in the second case it situated onto the bottom wall and lastly in the third case; right side of the vertical is heated. The implications of varying the Rayleigh numbers *Ra*, Hartmann number *Ha* and physical parameters for the system are the cavity aspect ratio *AR* will be emphasized. The results are presented in terms of streamline and isotherm patterns at the three different regimes of flow $Ra = 10^3$, 10^4 and 10^5. Prandtl number is chosen as Pr = 7.1 and Reynolds number is fixed at Re = 100. The variations of the average Nusselt number at the heated surface, average fluid temperature at the exit port and pressure and temperature gradient in the domain for the different values of the parameters.

3.1 CASE 1

Fig. 3.1 shows the effect of Hartmann number on the streamlines (on the left) and isotherms (on the right) at $Ra = 10^3$ and AR = 1. It is clearly seen from the figures, heating part of the cavity is not so effective on flow distribution and inlet flow goes through the channel from the top wall of the channel without any circulation inside the cavity except Ha = 0. This is because the lower value of Rayleigh number. One may notice that a circulating cell is formed in the clockwise direction and $\psi_{min} = -0.001$ at the bottom part of the cavity in absence of magnetic field. Isotherms are distributed from the left heated vertical wall into the cavity and hot fluid leave from the cavity from right top side. The effect of Hartmann number on the flow field and temperature fields has been depicted in Fig 3.2 at $Ra = 10^4$ and AR = 1. We observe that the flow and temperature fields are almost same as Fig. 3.1 for higher values Hartmann number Ha (= 50 and 100). But, an interesting result is found that a

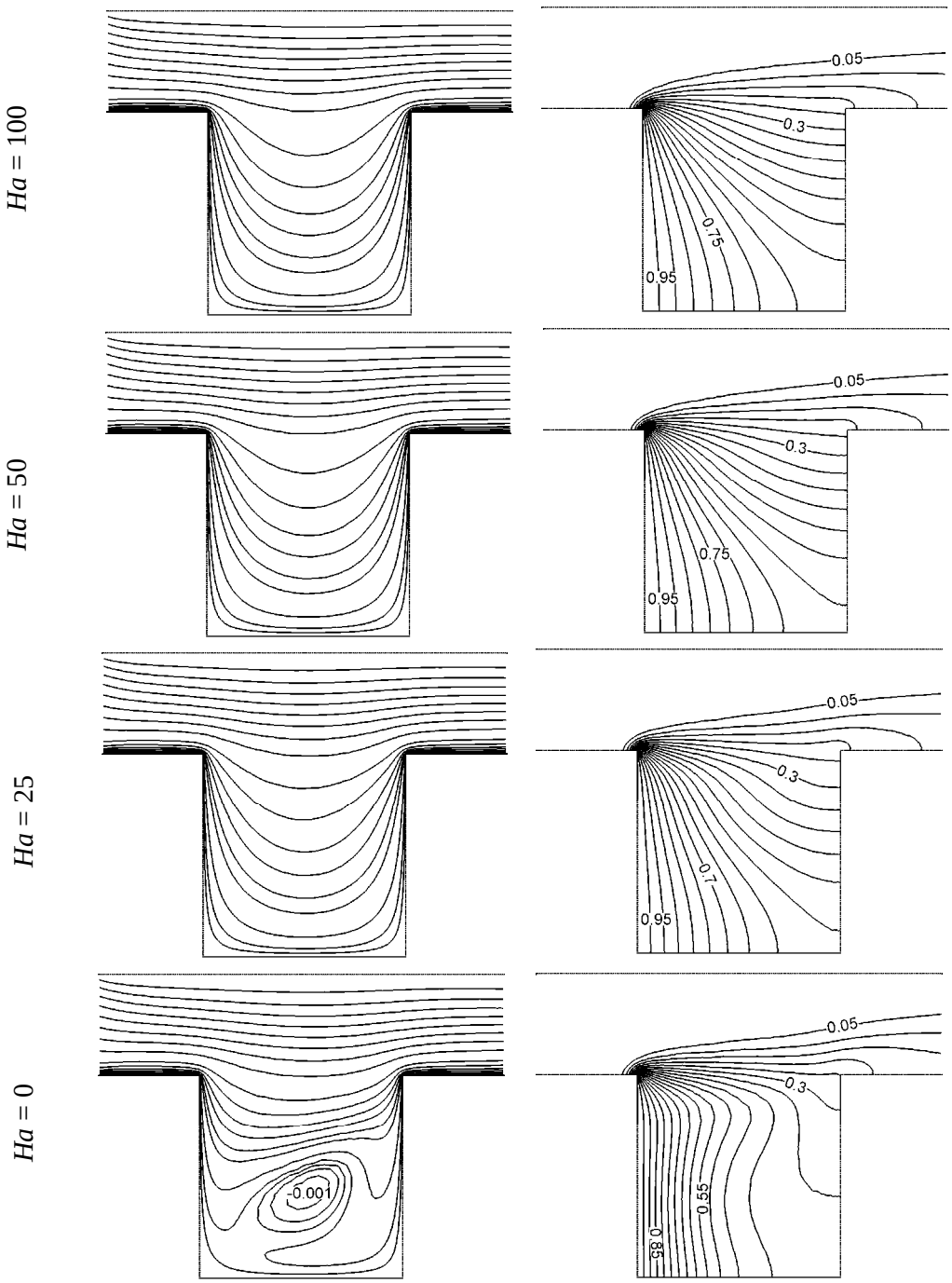

Fig. 3.1 (a) Streamlines and (b) Isotherms for the case 1 at $Ra = 10^3$, $AR = 1$ and selected values of Hartmann number Ha.

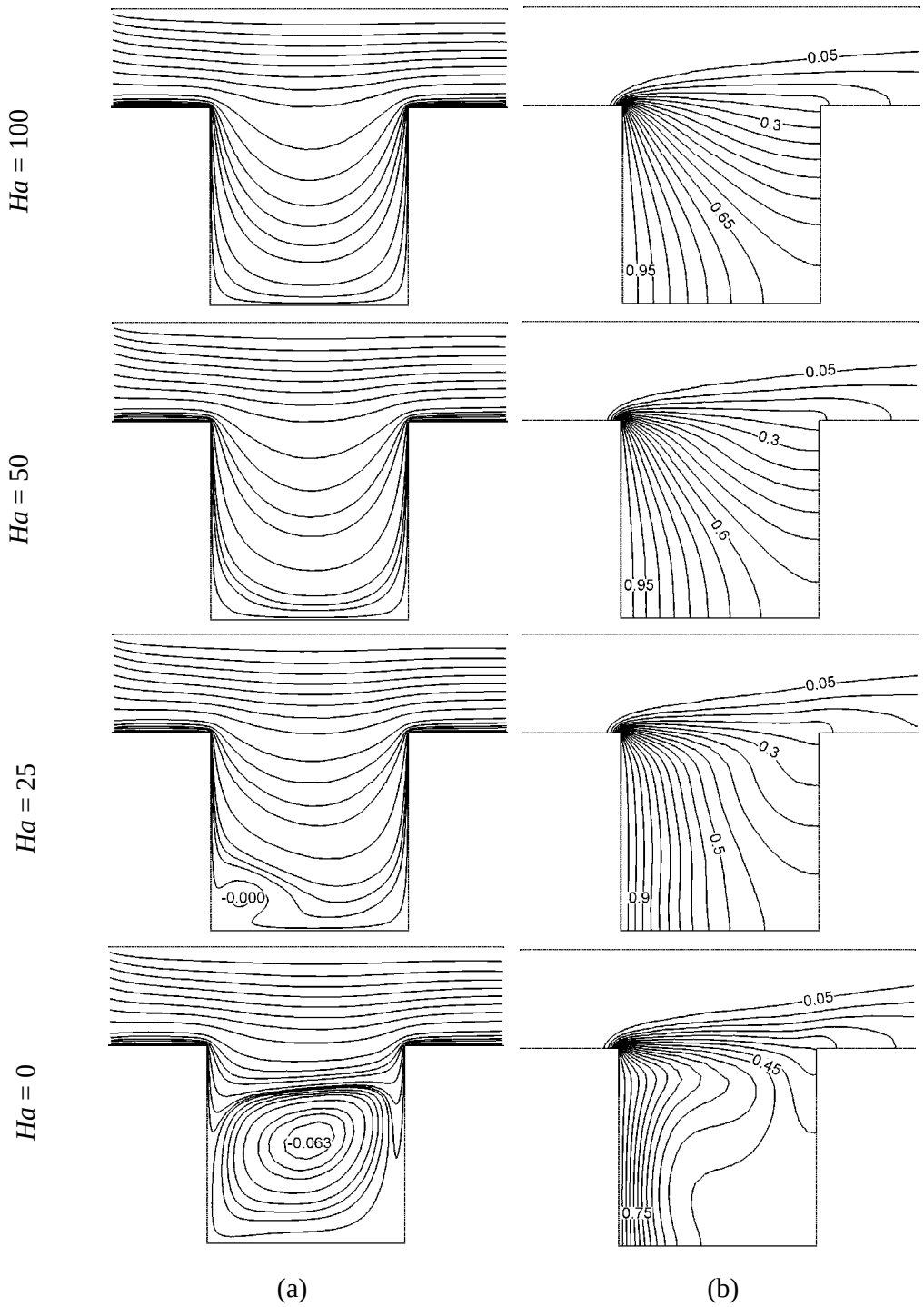

Fig. 3.2 (a) Streamlines and (b) Isotherms for the case 1 at $Ra = 10^4$, $AR = 1$ and selected values of Hartmann number Ha.

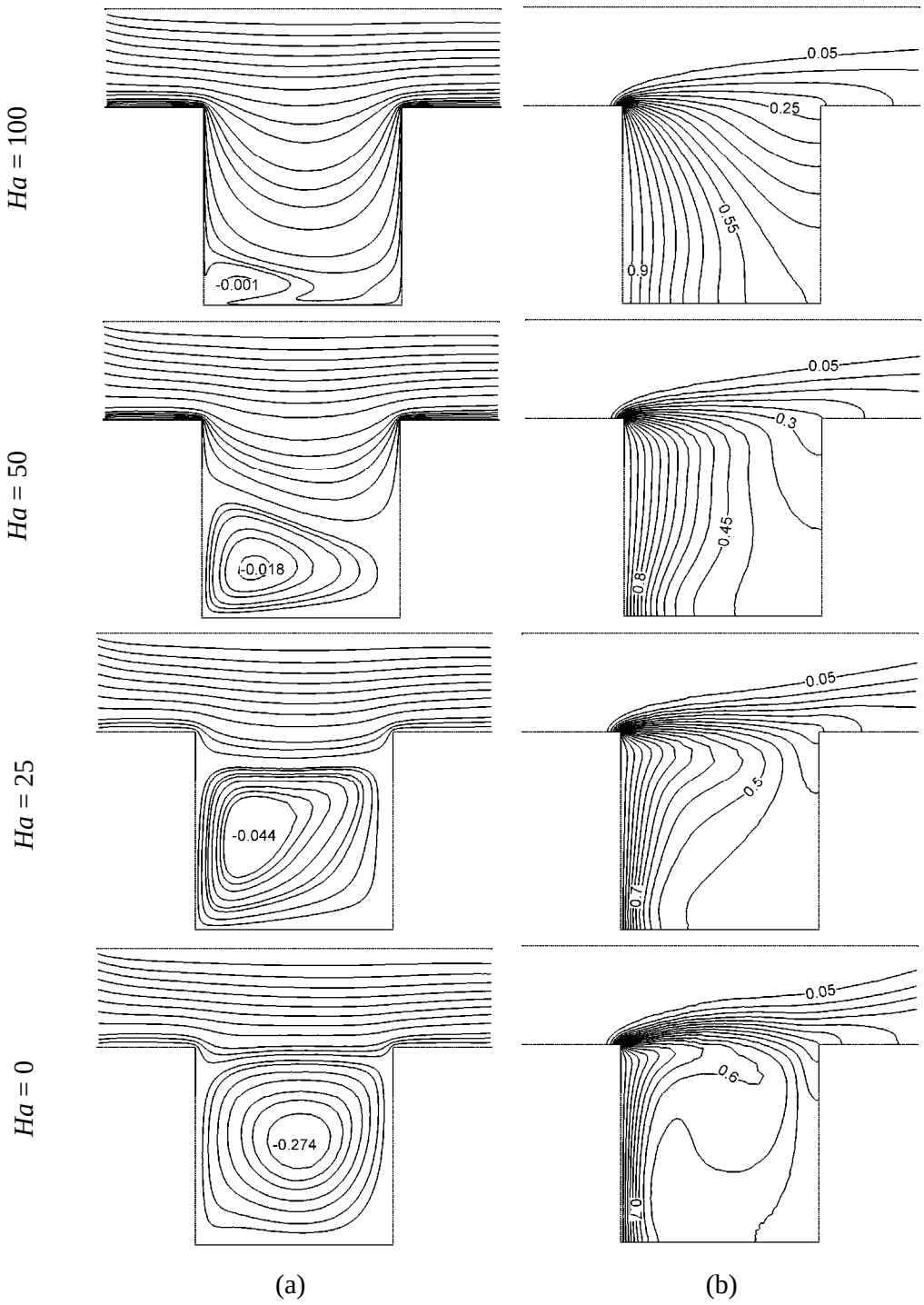

Fig. 3.3 (a) Streamlines and (b) Isotherms for the case 1 at $Ra = 10^5$, $AR = 1$ and selected values of Hartmann number *Ha*.

circulating cell is formed in the clockwise direction and ψ_{min} = -0.063 in absence of magnetic field. It is also noticed that the clockwise rotating cell covered most of the part of the cavity. As the cavity is heated from the left wall, the cavity behaves like differentially heated cavity from left and right. Thus, isotherms are parallel to left wall and wavy distribution is formed. The influence of Hartmann number on the streamlines and isotherms has been displayed in Fig 3.3 at Ra = 10^5 and AR = 1. One may notice that both the flow field as well as the thermal field strongly influenced for higher values of Rayleigh number. It can easily be seen that the circulating cell is formed in the clockwise direction and ψ_{min} = -0.274 in absence of magnetic field. If this figure is compared with Fig. 3.1, the circulation cell becomes stronger with ψ_{min} = -0.274 at Ha = 0. It is also noticed that the clockwise rotating cell occupies almost whole of the part of the cavity. This clockwise circulating cell decreases with the increasing values of Hartmann number. The location of the main center is changed a little bit to right side. The circulating cell center move to vertical heated. It is also clearly seen that the shape and size of the eddy changes while magnetic force changes. For Ra = 10^5, thermal boundary layer becomes thinner due to higher values of Rayleigh number as seen from Fig. 3.3. Plume like temperature distribution is seen for Ha = 0. Isotherms are parallel to the heater for Ha = 100 due to low flow velocity. In this case, isotherms are clustered around the heater and fluid flows directly over the cavity. Because domination of buoyancy effective flow is increased. Figs. 3.4 – 3.6 presents the outcome of Hartmann number on the streamlines (on the left) and isotherms (on the right) while AR = 2. Fig. 3.4 shows the streamline (on the left) and isotherms (on the right) for different values of Hartmann numbers at Ra = 10^3. In this cases, heating part of the cavity does not an effective parameter on the flow field and inlet flow goes through the channel from the top wall of the channel without any circulation inside the cavity apart from Ha = 0. For Ha = 0, a very small circulation cell with clockwise rotating direction is formed at right bottom corner of the cavity due to domination of buoyancy force. Fig. 3.4 (on the right) illustrates the isotherms to see the effects of temperature distribution with different magnetic forces. Isotherms are spread from the right heated vertical wall into the cavity and hot fluid go away from the cavity from right top side. As seen from the figure, thermal boundary layer becomes thicker with decreasing of Hartmann number.

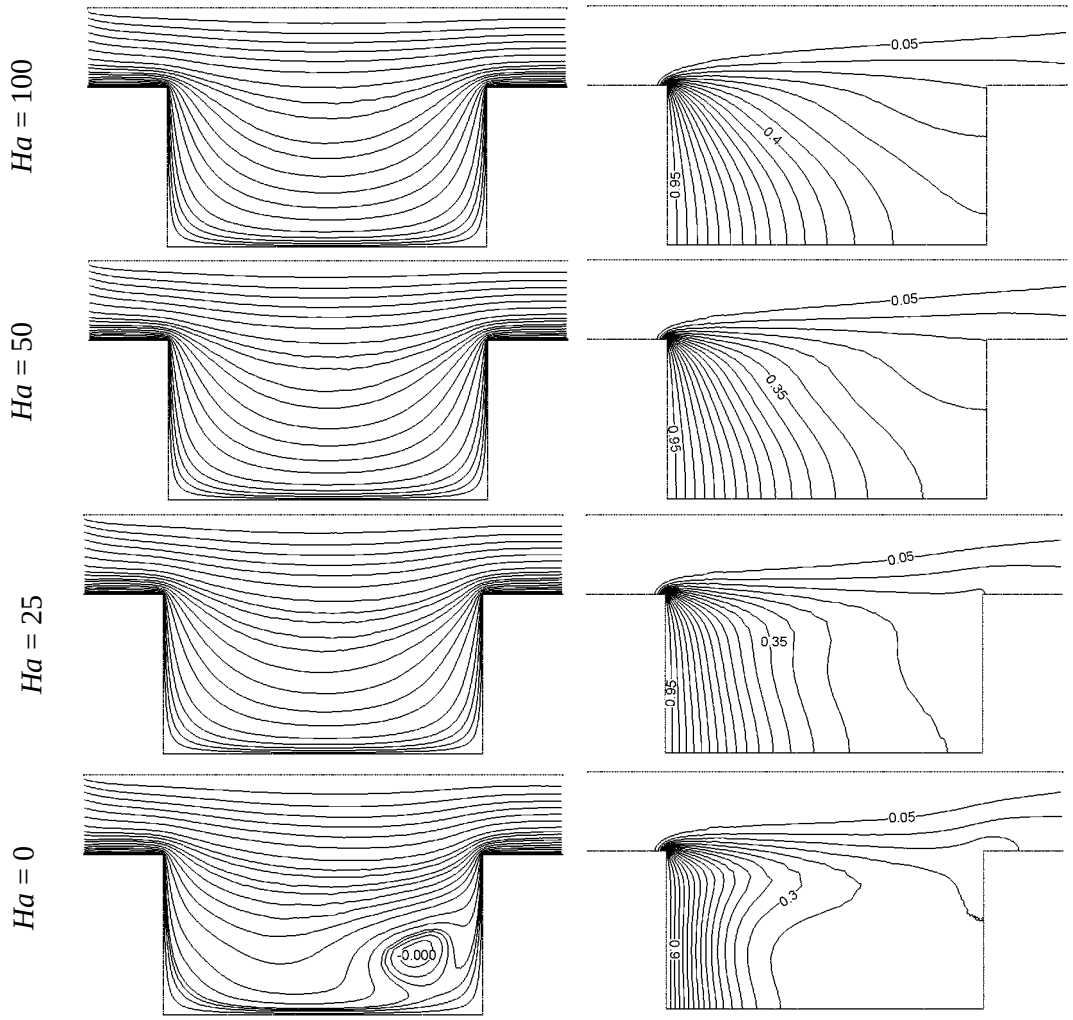

Fig. 3.4 (a) Streamlines and (b) Isotherms for the case 1 at $Ra = 10^3$, $AR = 2$ and selected values of Hartmann number *Ha*.

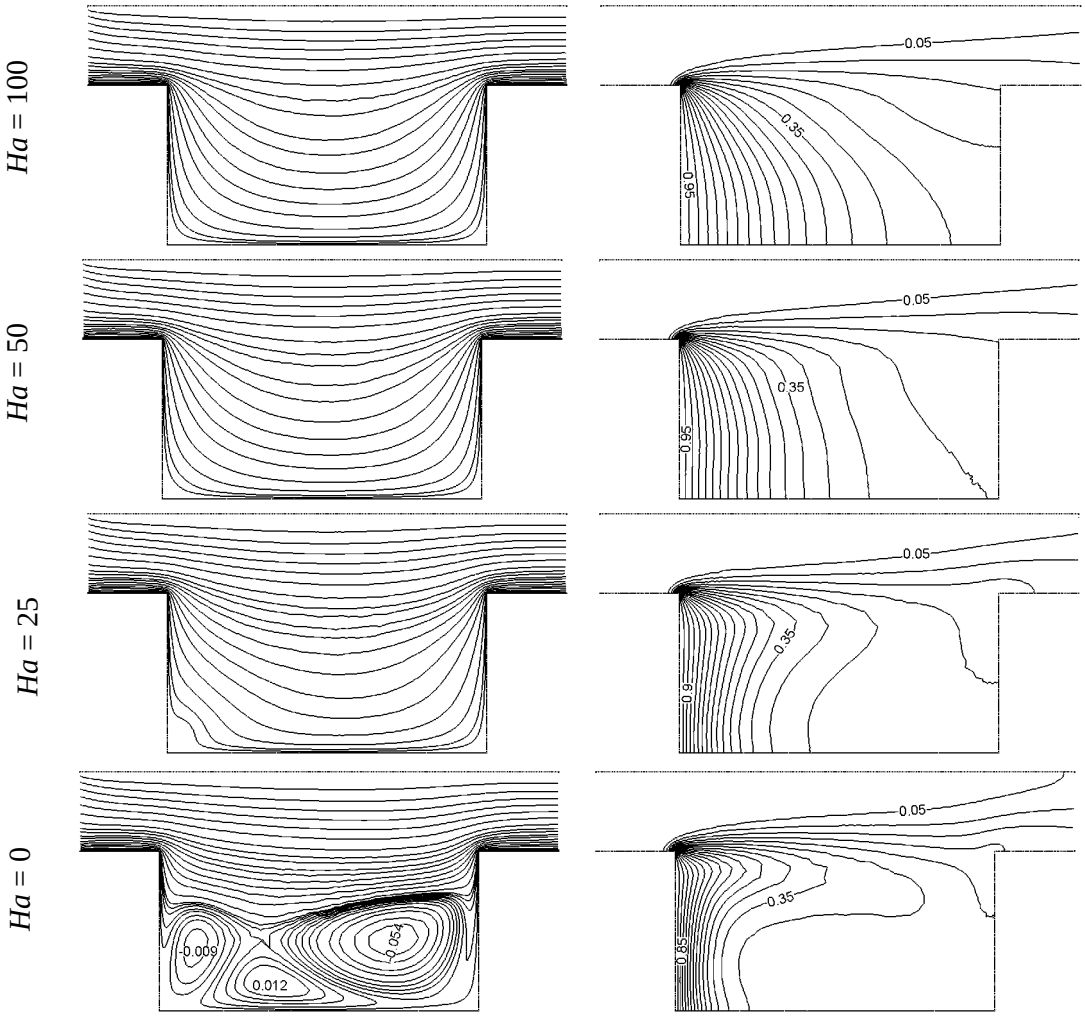

Fig. 3.5 (a) Streamlines and (b) Isotherms for the case 1 at $Ra = 10^4$, $AR = 2$ and selected values of Hartmann number *Ha*.

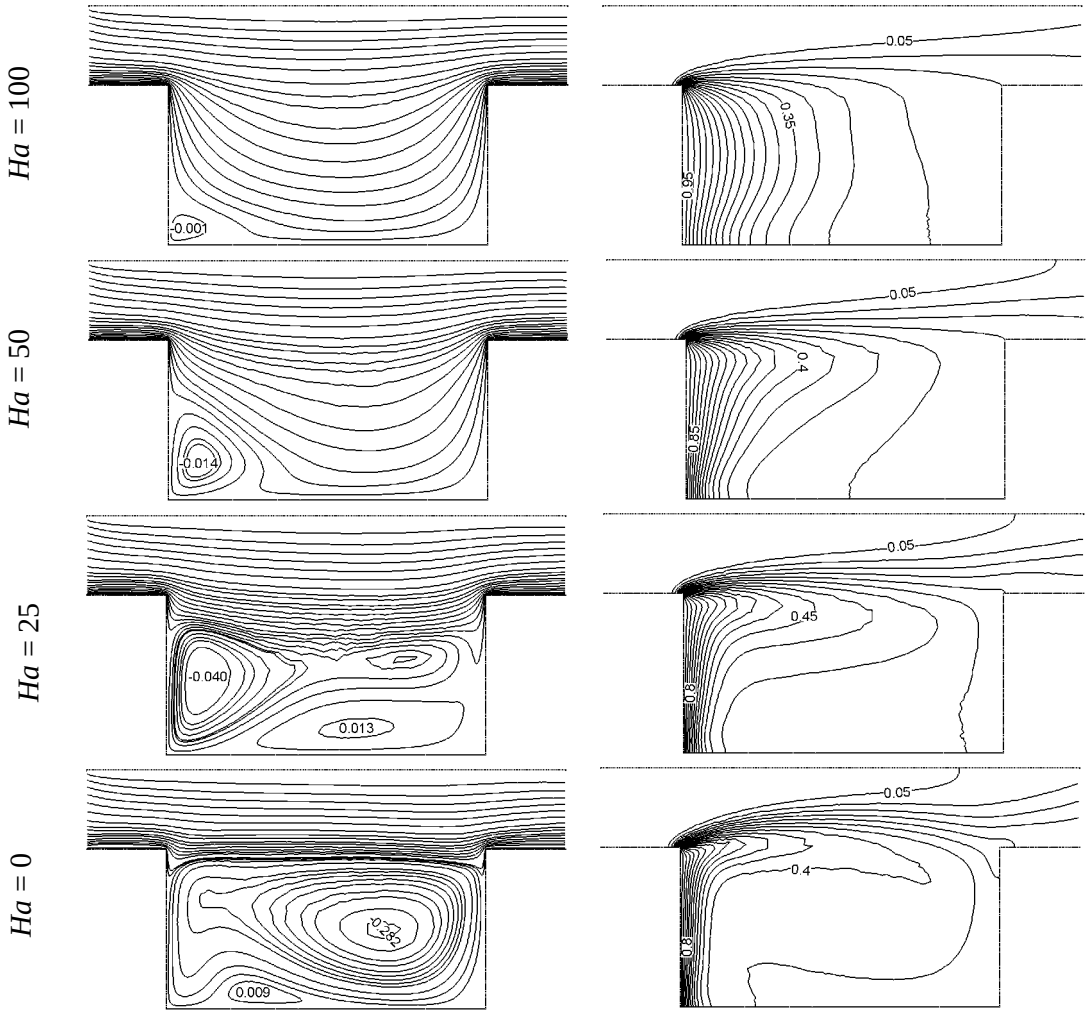

Fig. 3.6 (a) Streamlines and (b) Isotherms for the case 1 at $Ra = 10^5$, $AR = 2$ and selected values of Hartmann number Ha.

The effect of Hartmann number on the flow field and temperature fields has been shown in Fig 3.5 at Ra = 10^4 and AR = 2. It can be seen that the flow and temperature fields are almost identical as Fig. 3.4 for higher values Hartmann number Ha (= 25, 50 and 100). But, an interesting result is found that three circulating cells is formed in absence of magnetic field. As seen from the figure, thermal layer becomes thicker with decreasing of Hartmann number. For Ha = 0, plume like distribution is formed. Fig. 3.6 is plotted streamlines and isotherms for different values of Hartmann number *Ha* = 0, 25, 50 and 100 at Ra = 10^5. As seen from the left column of this figure, an amount of fluid near the heating wall of the cavity is activated so as to create a buoyancy-induced clockwise rotating cell for the lowest value of *Ha* = 0. As the Hartmann number increases the strength of the rotating cell is reduced and pushed to the left bottom corner of the cavity and then through flow in the channel gains its strength and occupies the whole of the cavity as well as the channel indicating the establishment of conduction mode of heat transfer. A higher value of Hartmann number, which is a measure of magnetic field, retards the flow velocity. Thus, this recirculation cell becomes smaller at Ha = 50, and 100 and it disappeared for further values of magnetic field. The corresponding isotherms for the lowest value of *Ha* = 10 shows the usual convective twist inside the cavity. The distortion of isothermal lines appears due to the high convective current inside the cavity. Distortions of isothermal lines start to disappear with increasing Hartmann number. As Hartmann number increases, isothermal lines inside the cavity as well as the channel approaches more and more towards the conduction-like distribution pattern of isothermal lines. For large Hartmann number *Ha* = 50 and 100, the convection is almost suppressed, and the isotherms are almost parallel to the horizontal wall, indicating that a quasiconduction regime is reached. Plume like temperature distribution is seen for Ha = 0 and 25.

Fig. 3.7 (a) and (b) illustrate the average Nusselt number and average fluid temperature at the exit port, respectively while AR = 1. The figures are given for different Rayleigh numbers at selected values of Hartmann numbers. Both Nusselt number and average fluid temperature at the exit port exhibit similar trends. In addition, both heat transfer and average fluid temperature are decreased with increasing of Hartmann numbers.

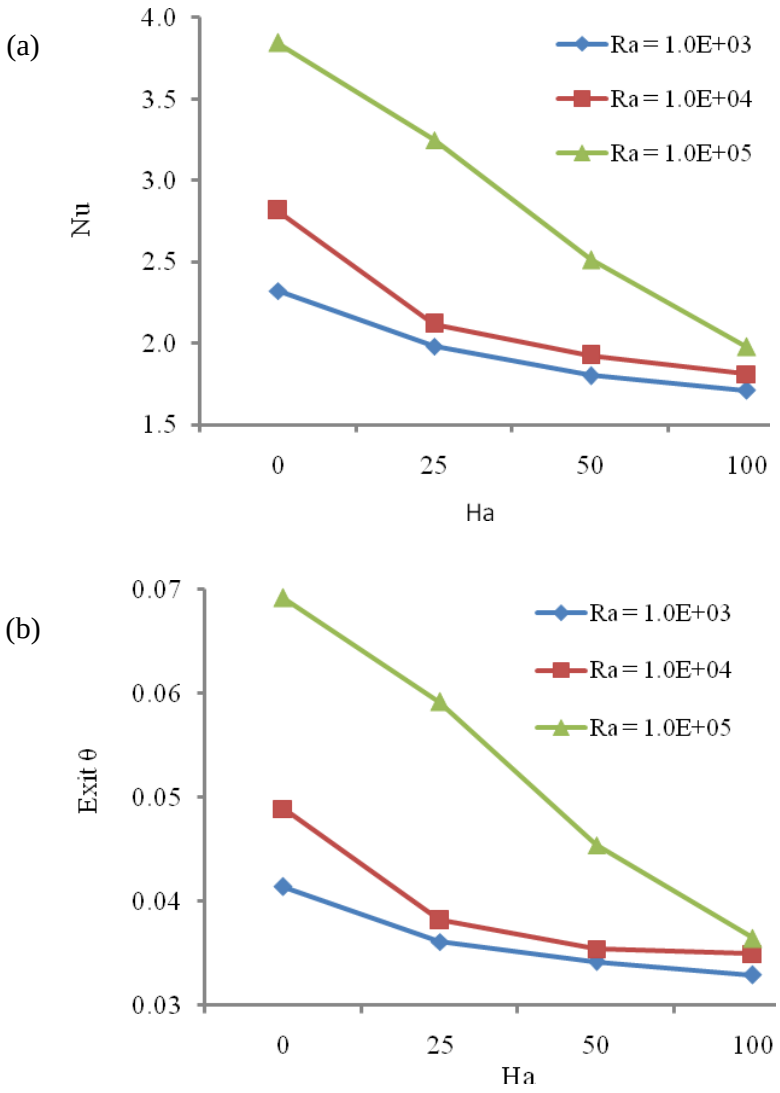

Fig. 3.7 (a) Average Nusselt number and (b) average fluid temperature at the exit port versus Hartmann number *Ha* for the case 1, at *AR* = 1 and selected values of Rayleigh number *Ra*.

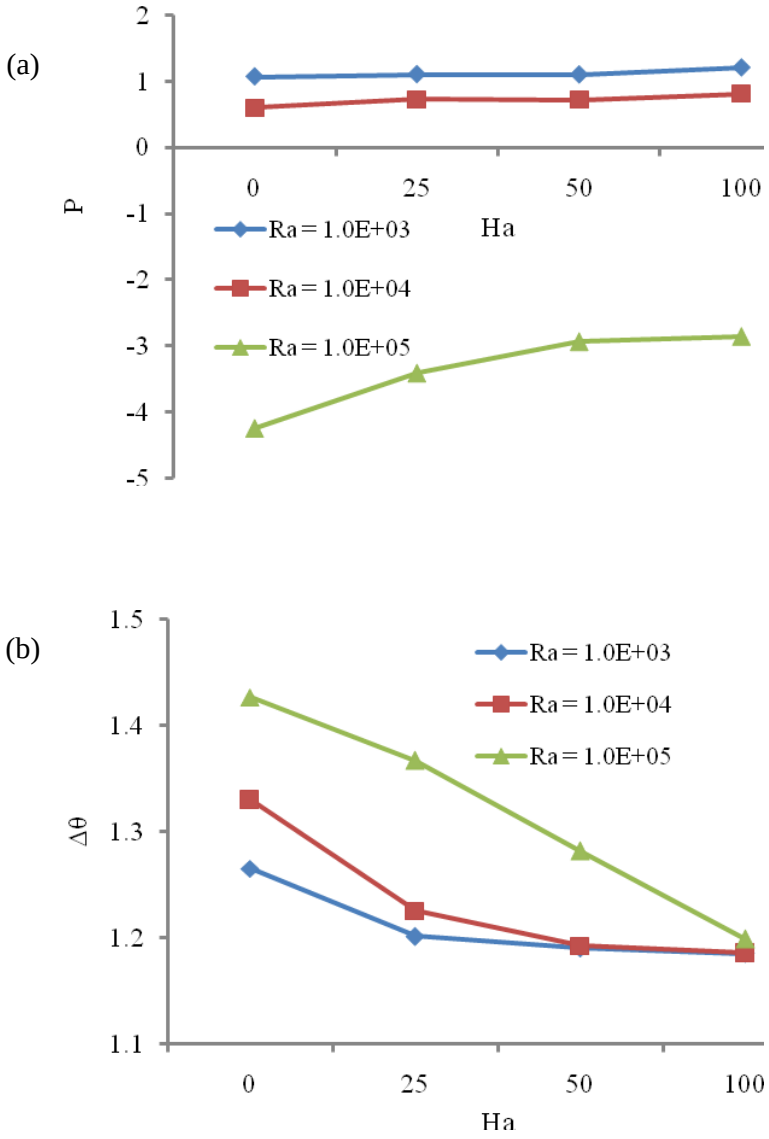

Fig. 3.8 (a) Pressure and (b) temperature gradient in the domain versus Hartmann number *Ha* for the case 1, at *AR* = 1 and selected values of Rayleigh number *Ra*.

(a)

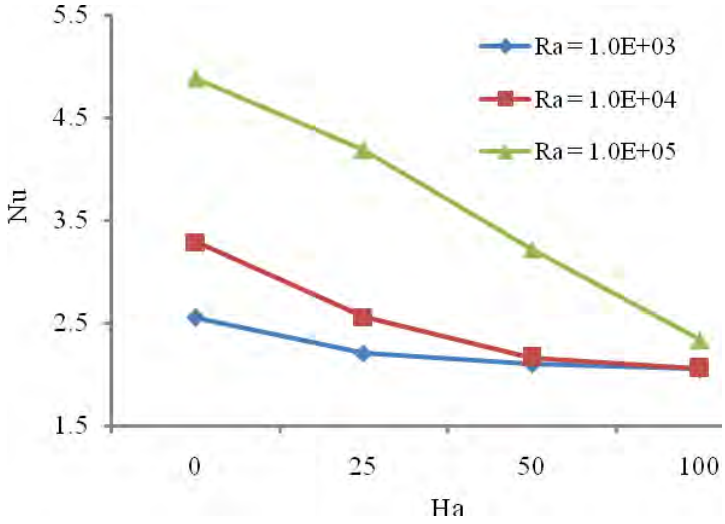

(b)

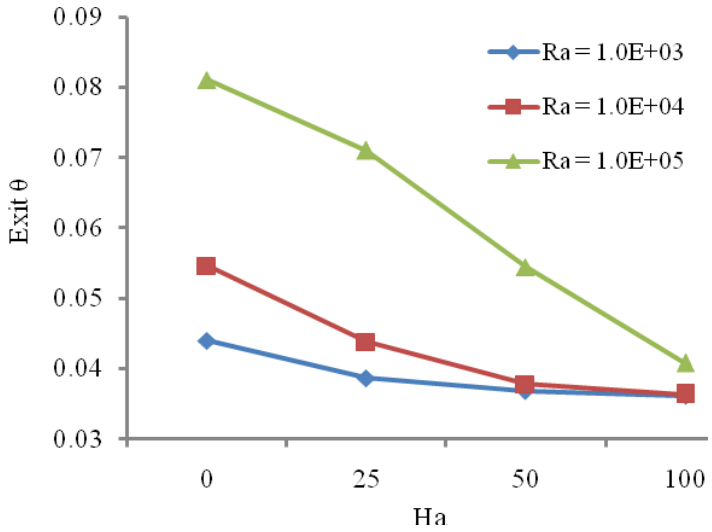

Fig. 3.9 (a) Average Nusselt number and (b) average fluid temperature at the exit port versus Hartmann number *Ha* for the case 1, at *AR* = 2 and selected values of Rayleigh number *Ra*.

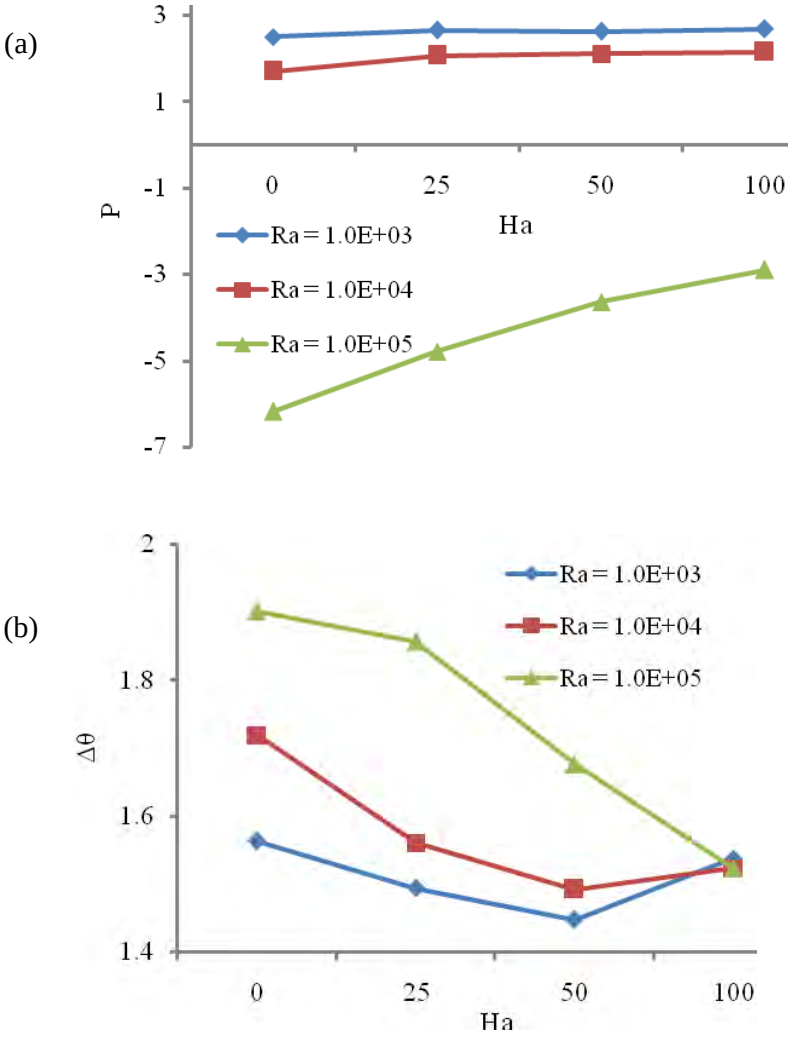

Fig. 3.10 (a) Pressure and (b) temperature gradient in the domain versus Hartmann number *Ha* for the case 2, at *AR* = 2 and selected values of Rayleigh number *Ra*.

Heat transfer becomes constant for Ra = 10^3, 10^4 and 10^5 due to decreasing of flow velocity with increasing of strength of magnetic field.

Pressure and temperature gradient in the domain for different Rayleigh number while AR = 1 is presented in Fig. 3.8. It is seen that pressure is almost zero up to Ra = 10^4 but negative values are formed for increasing of Rayleigh number. Also, temperature gradient is presented in Fig. 3.8 (b). As seen from the figure, general view of temperature gradient exhibit decreasing behavior with Rayleigh number. It is noticed that temperature becomes constant for Ra = 10^3 and 10^4 between Ha = 50 and Ha = 100 as given in Fig. 3.8 (b).

Variation of average Nusselt number and average fluid temperature at the exit port have been depicted in Fig. 3.9 (a) and (b), respectively while AR = 2. Both Nusselt number and average fluid temperature at the exit port reveal comparable trends. Additionally, both heat transfer rate and average fluid temperature are decreased with escalating of Hartmann numbers. One may notice that heat transfer rate decreases very smoothly Ra = 10^5 with increasing of strength of magnetic field.

On the other hand, pressure and temperature gradient in the domain for different Rayleigh number while AR = 2 is presented in Fig. 3.10. It is seen that pressure is positive up to Ra = 10^4 but negative values are produced for increasing of Rayleigh number. Also, temperature gradient is shown in Fig. 3.10(b). It is clearly seen from the figure, general view of temperature gradient demonstrates decreasing behavior with Rayleigh number. However, the temperature gradient increases for Ra = 10^3 and 10^4 between Ha = 50 and Ha = 100.

3.2 CASE 2

In this case, heater is located onto the bottom wall of the enclosure. Fig. 3.11 illustrates the effect of Hartmann number on the streamlines (on the left) and isotherms (on the right) at Ra = 10^3 and AR = 1. It can easily be seen from the figures, heating part of the cavity is not so effective on flow distribution and inlet flow goes through the channel from the top wall of the channel without any circulation inside the cavity excluding Ha = 0. This is because the lower value of Rayleigh number. A circulating cell is fashioned in the clockwise direction and ψ_{min} = -0.002 at the bottom part of the cavity in absence of magnetic field. Isotherms are

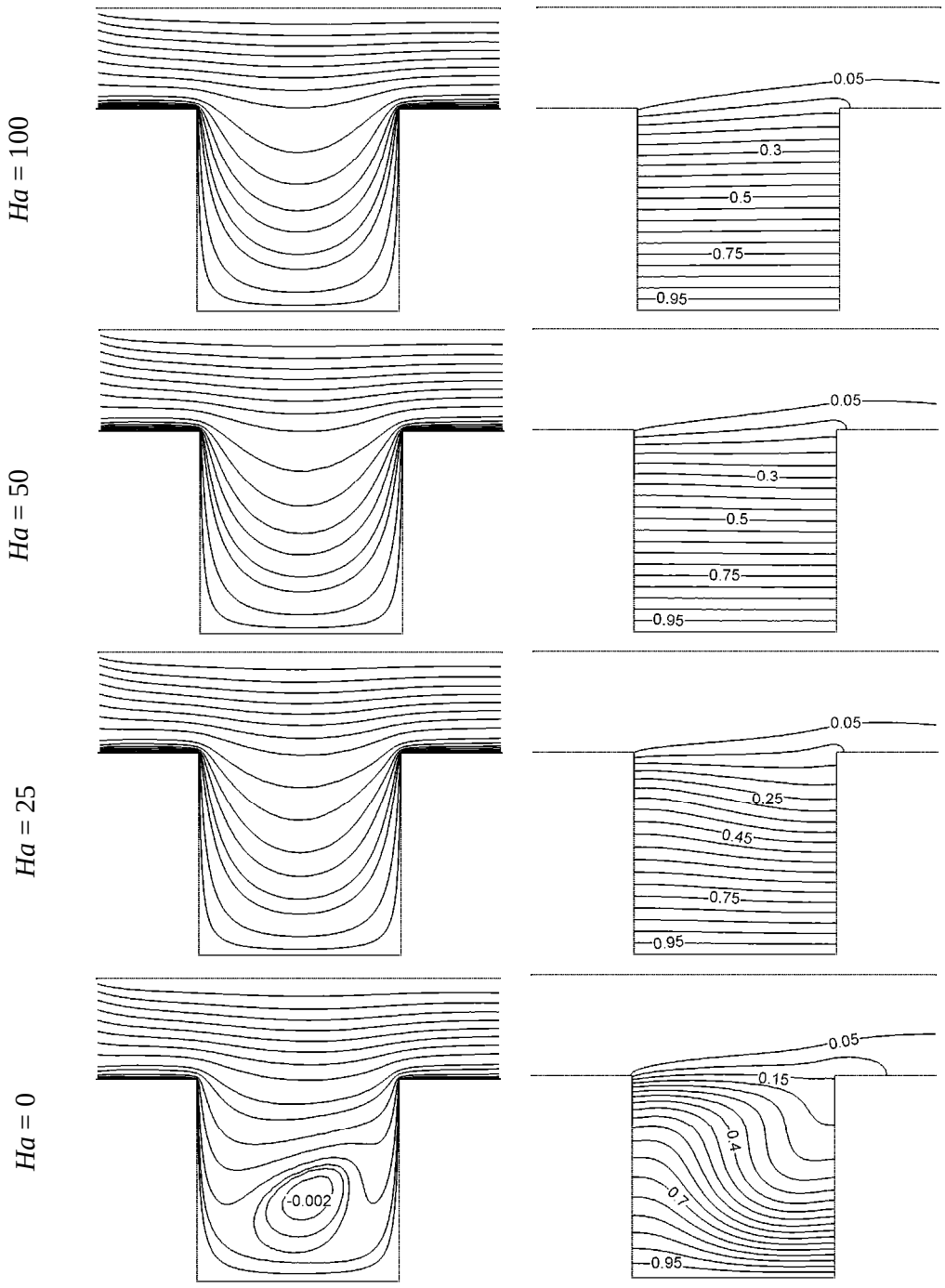

Fig. 3.11 (a) Streamlines and (b) Isotherms for the case 2 at $Ra = 10^3$, $AR = 1$ and selected values of Hartmann number Ha.

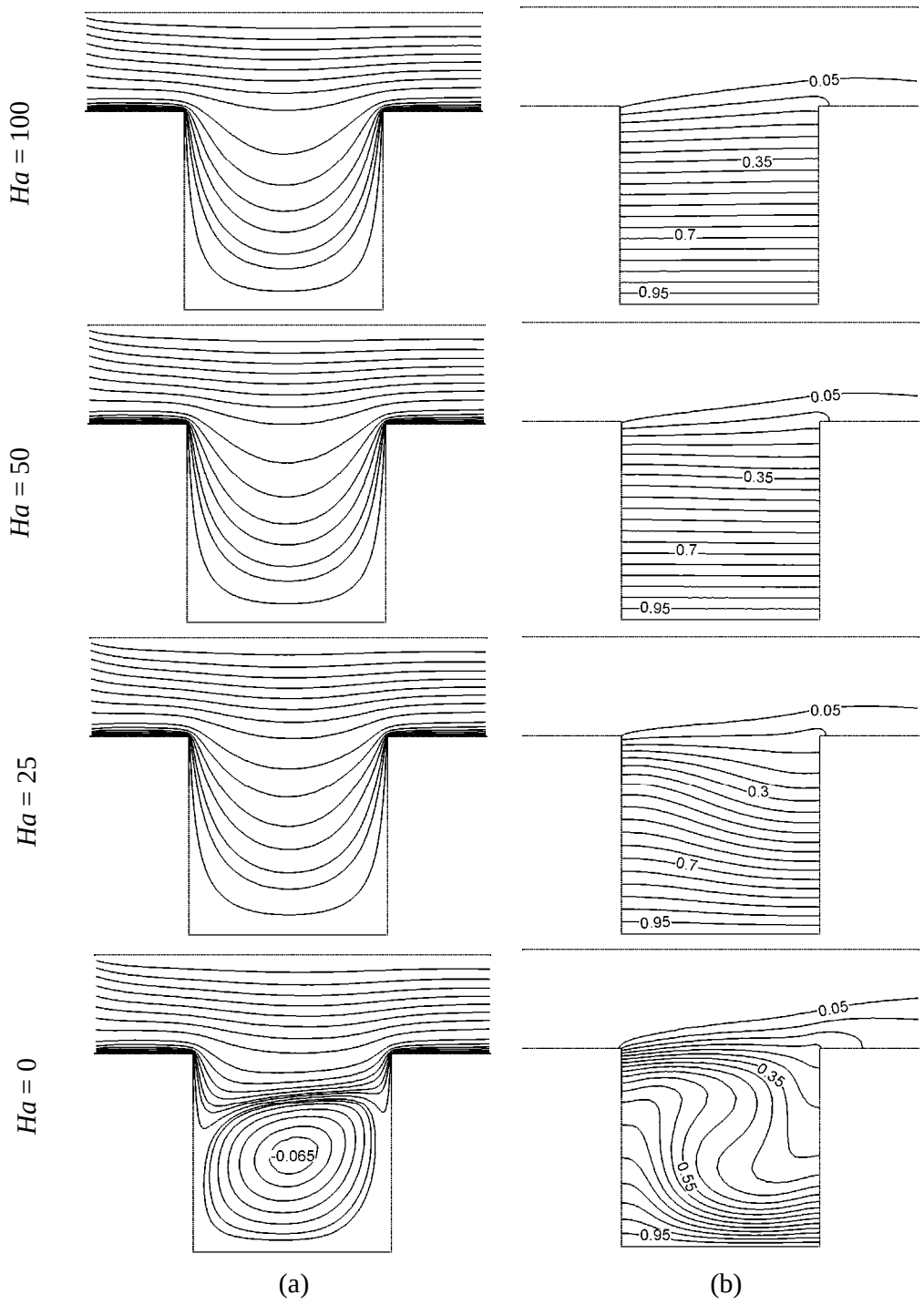

Fig. 3.12 (a) Streamlines and (b) Isotherms for the case 2 at $Ra = 10^4$, $AR = 1$ and selected values of Hartmann number Ha.

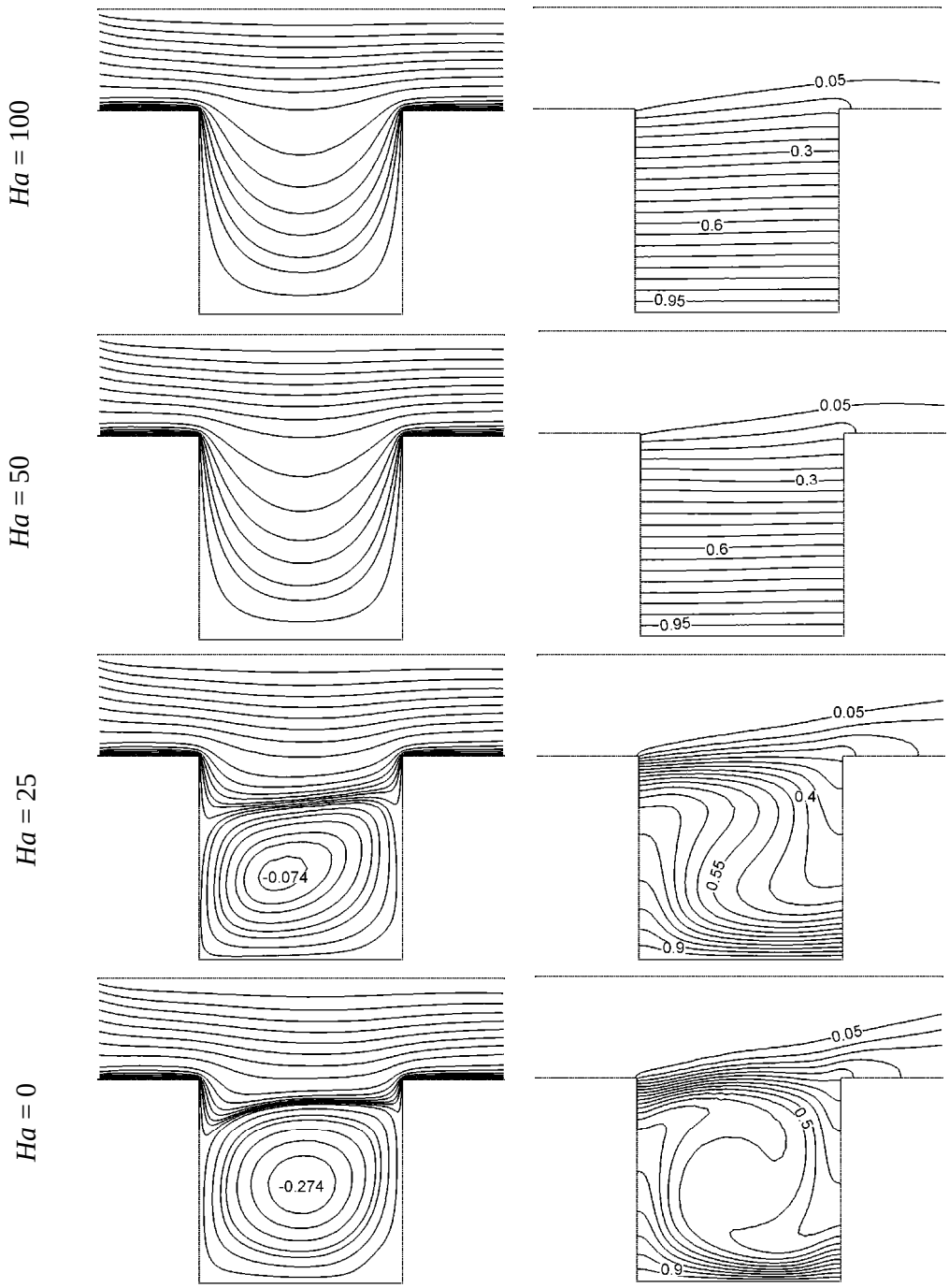

Fig. 3.13 (a) Streamlines and (b) Isotherms for the case 2 at $Ra = 10^5$, $AR = 1$ and selected values of Hartmann number Ha.

distributed from the bottom heated wall into the cavity and hot fluid leave from the cavity from right top side. Isotherms are almost parallel to the bottom surface. The effect of Hartmann number on the flow field and temperature fields has been shown in Fig 3.12 at Ra = 10^4 and AR = 1. It is clearly seen that the flow and temperature fields are almost same as Fig. 3.11 for higher values Hartmann number Ha (= 25, 50 and 100). But, an interesting result is found that a circulating cell is formed in the clockwise direction and ψ_{min} = -0.065 in absence of magnetic field. It is also noticed that the clockwise rotating cell enclosed the majority of the part of the cavity. Since the cavity is heated from the bottom wall, the cavity behaves like differentially heated cavity from bottom and upper. Thus, isotherms are parallel to bottom wall and wavy distribution is produced. The outcome of Hartmann number on the flow field and temperature fields has been revealed in Fig 3.13 at Ra = 10^5 and AR = 1. It can easily be seen that the circulating cell is formed in the clockwise direction and ψ_{min} = -0.274 in absence of magnetic field. This clockwise rotating cell occupies almost whole of the part of the cavity. It is noticed that flow strength of core of the rotating cell decreasing with the escalating values of Hartmann number. And, also this cell disappears for higher magnetic field. For Ra = 10^5, thermal boundary layer becomes thinner due to higher values of Rayleigh number as seen from right column of Fig. 3.13. Isotherms are parallel to the heater for higher Ha (= 50 and 100) due to low flow velocity. However, spiral like temperature distribution is formed for lower Ha = (0 and 25).

Figs. 3.14 – 3.16 illustrates the effect of Hartmann number on the streamlines (on the left) and isotherms (on the right) while AR = 2. Fig. 3.14 displays the streamline (on the left) and isotherms (on the right) for different values of Hartmann numbers at Ra = 10^3. It is clearly be seen that heating part of the cavity does not influence on the flow field and flow goes through the channel from the top wall of the channel without any circulation inside the cavity in the presence of magnetic field. In absence of magnetic field, a very small circulation cell with clockwise rotating direction and ψ_{min} = -0.004 is formed at right bottom corner of the cavity due to domination of buoyancy force. Fig. 3.14 (on the right) shows the isotherms to analyze the effects of temperature distribution with different magnetic forces. Isotherms are spread from the bottom heated surface into the cavity and hot fluid leave from the cavity from

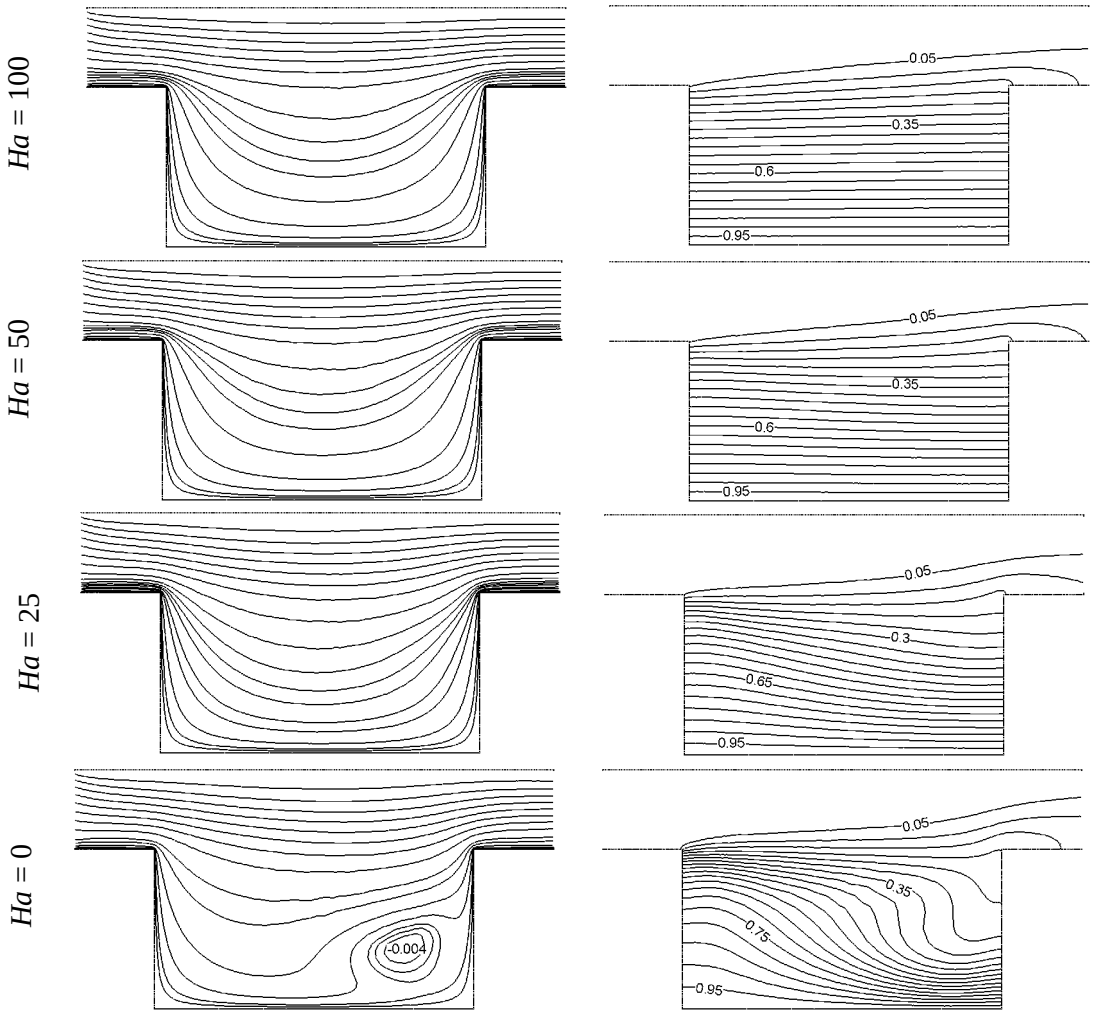

Fig. 3.14 (a) Streamlines and (b) Isotherms for the case 2 at $Ra = 10^3$, $AR = 2$ and selected values of Hartmann number Ha.

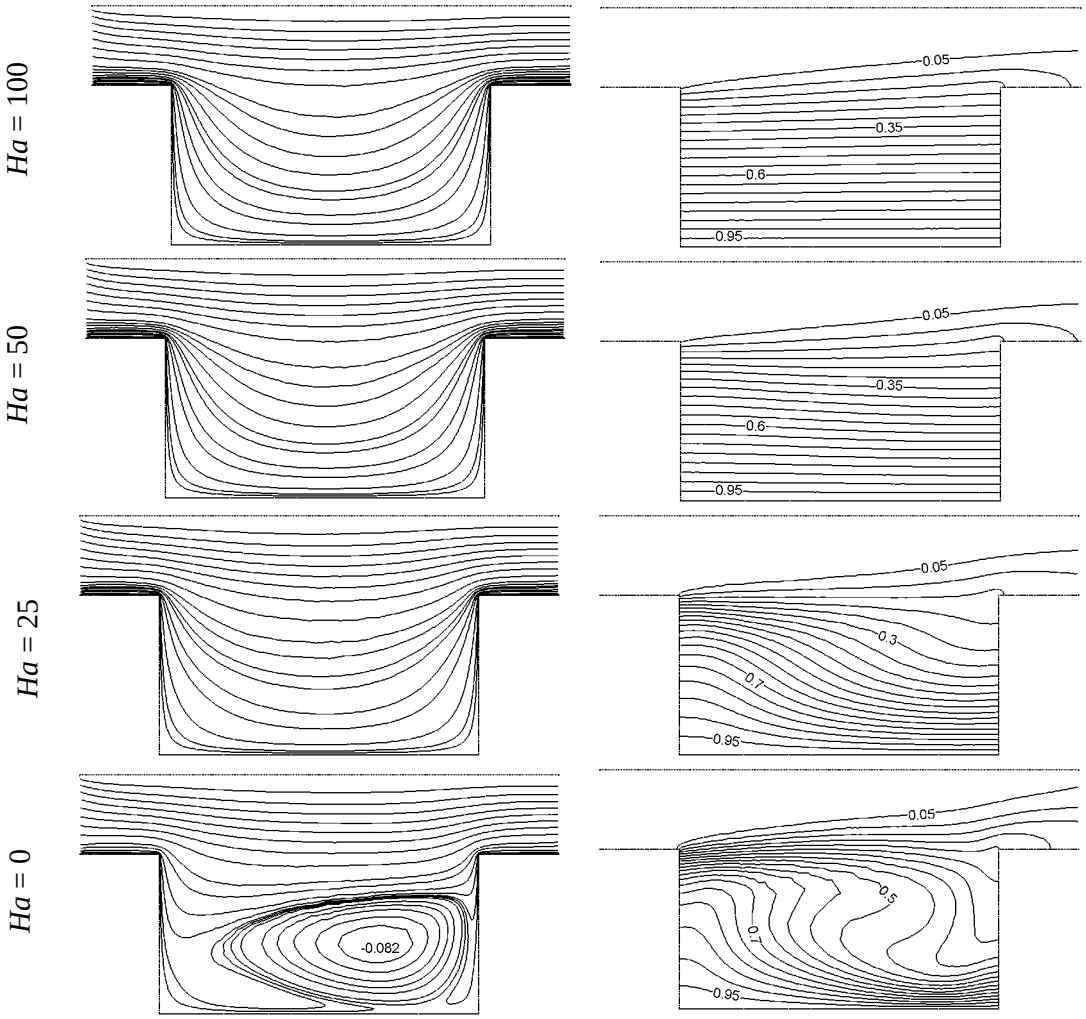

Fig. 3.15 (a) Streamlines and (b) Isotherms for the case 2 at $Ra = 10^4$, $AR = 2$ and selected values of Hartmann number Ha.

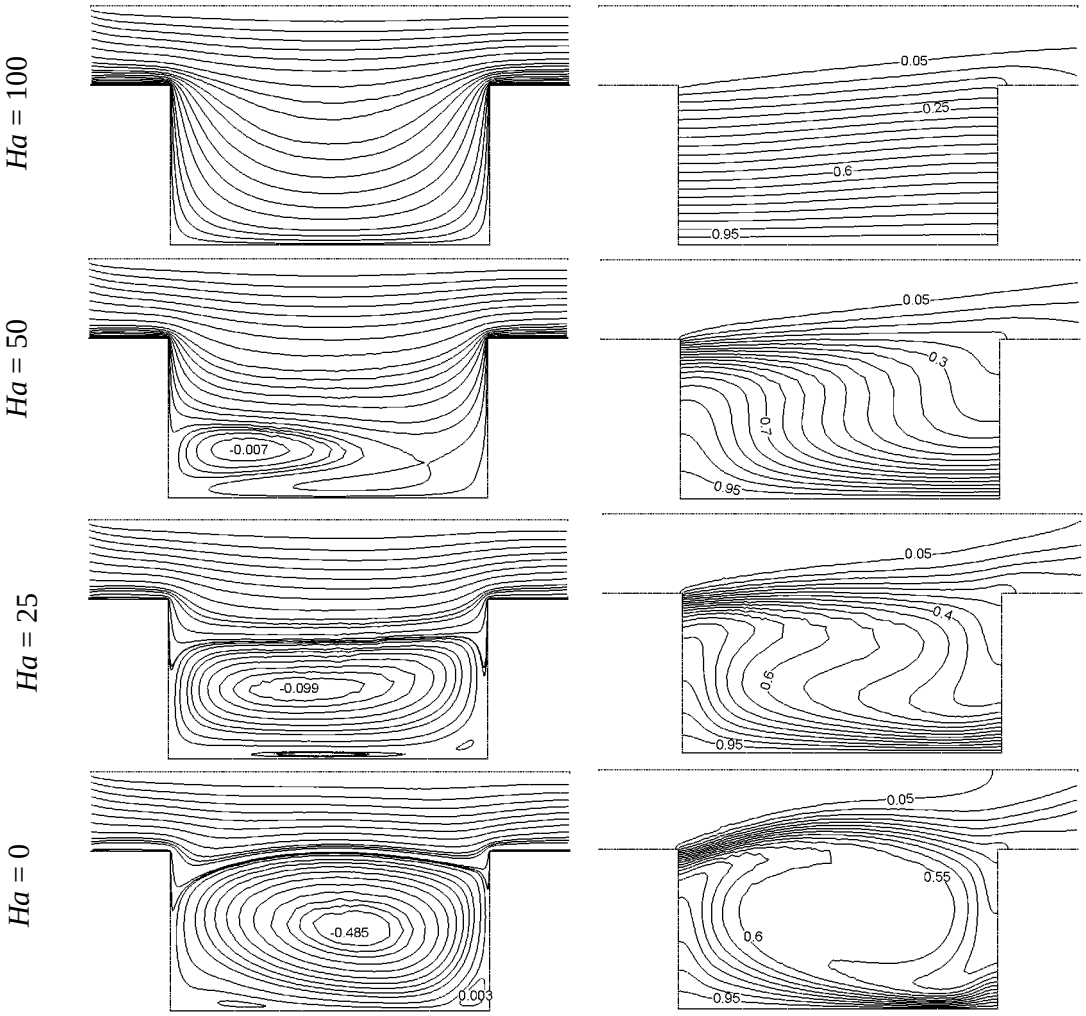

Fig. 3.16 (a) Streamlines and (b) Isotherms for the case 2 at $Ra = 10^5$, $AR = 2$ and selected values of Hartmann number Ha.

right top side. For large Hartmann number *Ha* = 50 and 100, the convection is almost suppressed, and the isotherms are almost parallel to the horizontal wall, indicating that a quasiconduction regime is reached. But wavy shaped isotherms are observed for lower values of Ha. The effect of Hartmann number on the flow field and temperature fields has been depicted in Fig 3.15 at Ra = 10^4 and AR = 2. It is found from the figure that the flow and temperature fields are almost indistinguishable as Fig. 3.14 for higher values Hartmann number Ha (= 25, 50 and 100). But, an interesting result is found that a circulating cell is formed in the clockwise direction and ψ_{min} = -0.002 at the bottom part of the cavity in absence of magnetic field. As seen from the figure, thermal layer becomes thicker with decreasing of Hartmann number. For Ha = 0, spiral like distribution is formed. Fig. 3.16 have been plotted streamlines and isotherms for different values of Hartmann number *Ha* = 0, 25, 50 and 100 at Ra = 10^5 and AR =2. As seen from the left column of this figure, an amount of fluid near the heating wall of the cavity is activated so as to generate a buoyancy-induced clockwise rotating cell for the lower values of *Ha* = (0, 25 and 50). As the Hartmann number increases the strength of the rotating cell is reduced and pushed to the left bottom corner of the cavity and then through flow in the channel gains its strength and occupies the whole of the cavity as well as the channel indicating the establishment of conduction mode of heat transfer. A higher value of Hartmann number, which is a measure of magnetic field, retards the flow velocity. Thus, this recirculation cell becomes smaller at Ha = 25, and 50 and it moved out for further values of magnetic field. In addition, the main flow suppresses the rotating flow inside the cavity. The corresponding isotherms for the lowest value of *Ha* = 0 shows the usual convective twist inside the cavity. The distortion of isothermal lines appears due to the high convective current inside the cavity. Distortions of isothermal lines start to disappear with increasing Hartmann number. As Hartmann number increases, isothermal lines inside the cavity as well as the channel approaches more and more towards the conduction-like distribution pattern of isothermal lines. For largest Hartmann number *Ha* = 100, the convection is almost censored, and the isotherms are almost parallel to the horizontal wall, indicating that a quasiconduction regime is reached. Wavy like temperature distribution is seen for Ha = 25 and 50.

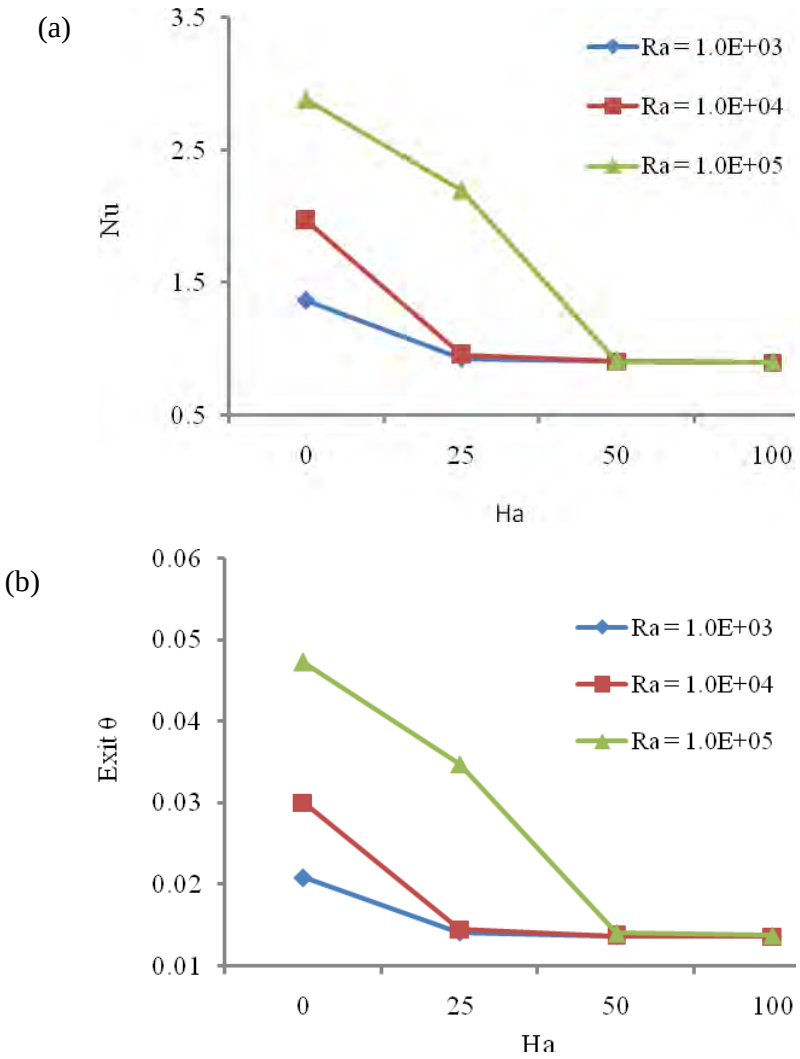

Fig. 3.17 (a) Average Nusselt number and (b) average fluid temperature at the exit port versus Hartmann number *Ha* for the case 2 at *AR* = 1 and selected values of Rayleigh number *Ra*.

(a)

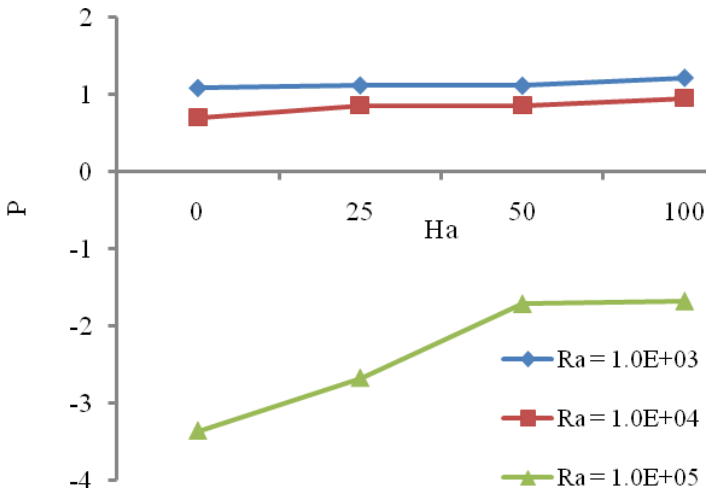

(b)

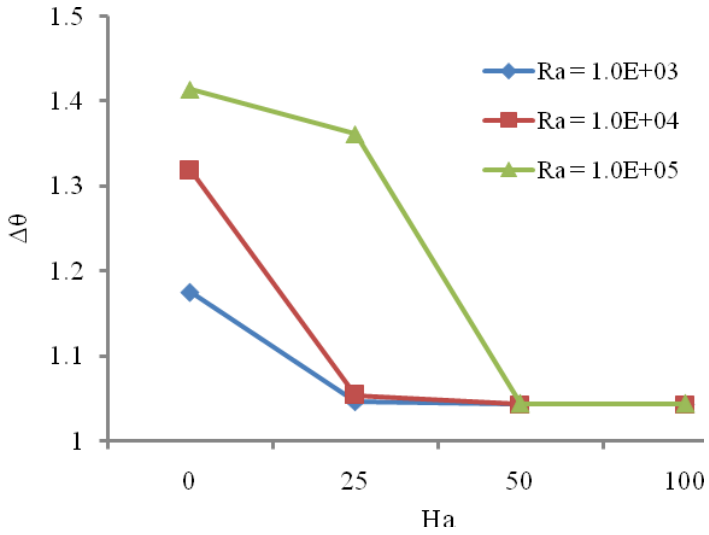

Fig. 3.18 (a) Pressure and (b) temperature gradient in the domain versus Hartmann number *Ha* for the case 1, at *AR* = 1 and selected values of Rayleigh number *Ra*.

(a)

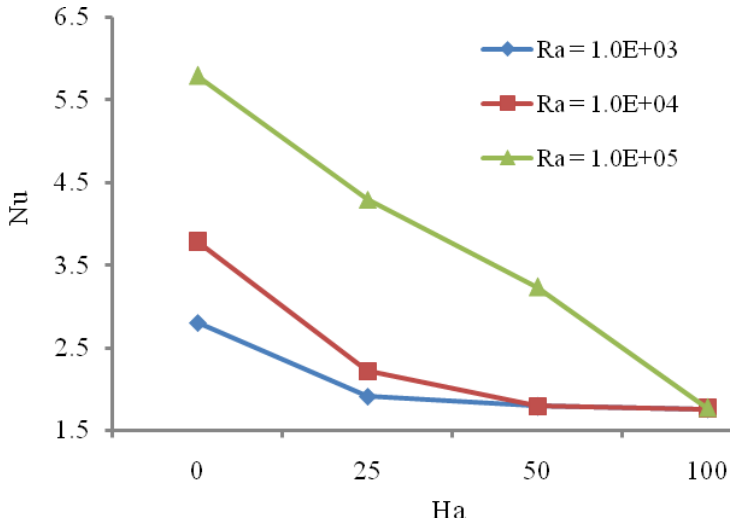

(b)

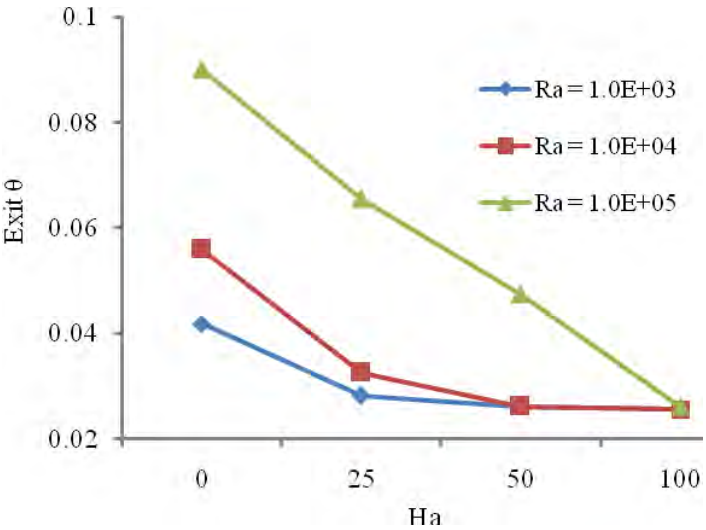

Fig. 3.19 (a) Average Nusselt number and (b) average fluid temperature at the exit port versus Hartmann number *Ha* for the case 2 at *AR* = 2 and selected values of Rayleigh number *Ra*.

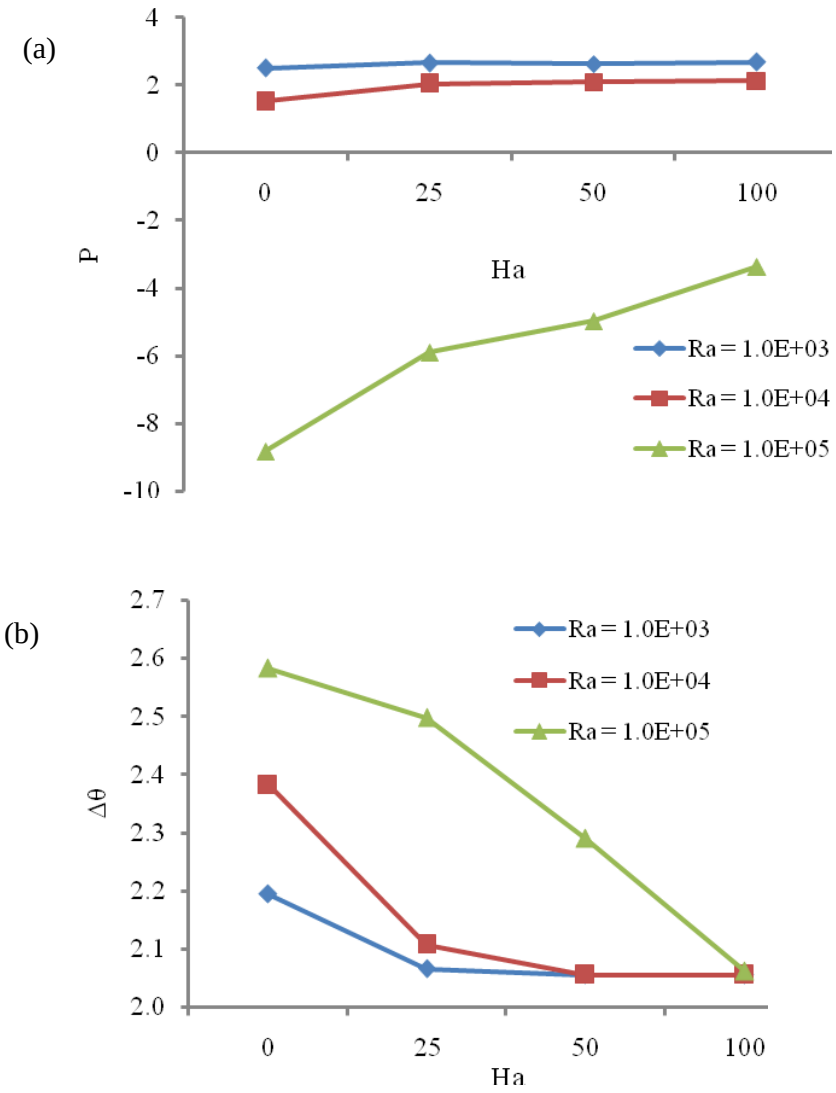

Fig. 3.20 (a) Pressure and (b) temperature gradient in the domain versus Hartmann number *Ha* for the case 2, at *AR* = 2 and selected values of Rayleigh number *Ra*.

Fig. 3.17 (a) and (b) express the average Nusselt number and average fluid temperature at the exit port, respectively while AR = 1. The figures are shown for different Rayleigh numbers at selected values of Hartmann numbers. Both Nusselt number and average fluid temperature at the exit port demonstrate comparable trends. In addition, both heat transfer and average fluid temperature are decreased with increasing of Hartmann numbers up to Ha = 50. Both heat transfer and average fluid temperature become steady for Ra = 10^3, 10^4 and 10^5 due to decreasing of flow velocity with increasing of strength of magnetic field. Pressure and temperature gradient in the domain for different Rayleigh number for AR = 1 is presented in Fig. 3.18. It is clearly seen that pressure is positive for lower values of Ra = 10^3 and 10^4, but negative values are formed for increasing of Rayleigh number. In addition, from Fig 3.18(a), one may notice that negative values of pressure decreases with decreasing of Hartmann numbers for Ra = 10^5. One the other hand, temperature gradient is offered in Fig. 3.18 (b). As seen from the figure, general view of temperature gradient exhibit decreasing behavior with increasing of Hartmann numbers up to Ha = 50. However, temperature gradient becomes constant for Ra = 10^3 and 10^4 from Ha = 25 to higher value, but for Ra = 10^5 from Ha = 50 to higher value.

Fig. 3.19 (a) and (b) presents the average Nusselt number and average fluid temperature at the exit port, respectively while AR = 2. The figures are displayed for different Rayleigh numbers at chosen values of Hartmann numbers. Both Nusselt number and average fluid temperature at the exit port show similar trends. Furthermore, both heat transfer and average fluid temperature are decreased with increasing of Hartmann numbers. A linear decreasing is seen for Ra = 10^5 with increasing of Hartmann number. This is because increasing of strength of magnetic field causes decreasing of flow velocity. Pressure and temperature gradient in the domain for different Rayleigh number for AR = 2 is depicted in Fig. 3.20. It is clearly seen that pressure is positive for lower values of Ra = 10^3 and 10^4. But negative values are found for increasing of Rayleigh number. Also, from Fig 3.20(a), it is easily seen that negative values of pressure decreases with decreasing of Hartmann numbers for Ra = 10^5. One the other hand, temperature gradient is

presented in Fig. 3.20 (b). As seen from the figure, broad view of temperature gradient exhibit decreasing behavior with increasing of Hartmann numbers.

3.3 CASE 3

Fig. 3.21 shows the effect of Hartmann number on the streamlines (on the left) and isotherms (on the right) at Ra = 10^3 and AR = 1. As seen from the figures, heating part of the cavity is not so effective on flow distribution and inlet flow goes through the channel from the top wall of the channel without any circulation inside the cavity. This is because the lower value of Rayleigh number. Isotherms are distributed from the right heated vertical wall into the cavity and hot fluid leave from the cavity from right top side. The cavity behaves like heated cavity from right. Thus, isotherms are parallel to right vertical wall and wavy distribution is formed in absence of magnetic field. The effect of Hartmann number on the flow field and temperature fields has been depicted in Fig 3.22 at Ra = 10^4 and AR = 1. It can easily be seen that the flow and temperature fields are just about similar as Fig. 3.21 for higher values Hartmann number Ha (= 25, 50 and 100). The influence of Hartmann number on the streamlines and isotherms has been displayed in Fig 3.23 at Ra = 10^5 and AR = 1. One may notice that both the flow field as well as the thermal field strongly influenced for higher values of Rayleigh number. It can easily be seen that a circulating cell is formed in the clockwise direction and ψ_{min} = -0.017 in absence of magnetic field at the bottom left corner. For Ra = 10^5, thermal boundary layer becomes thinner due to higher values of Rayleigh number as seen from Fig. 3.23. In this case, isotherms are clustered around the heater and fluid flows directly over the cavity. Because domination of buoyancy effective flow is increased.

Figs. 3.24 – 3.26 illustrates the streamlines (on the left) and isotherms (on the right) to see the effects of temperature distribution with different magnetic forces while AR = 2. Fig. 3.24 shows the streamline (on the left) and isotherms (on the right) for different values of Hartmann numbers at Ra = 10^3. The fluid flow is characterized by open lines and inlet flow goes through the channel from the top wall of the channel without any circulation inside the cavity. Besides, Fig. 3.25 illustrates the streamline (on the left) and isotherms (on the right) for different values of Hartmann numbers at Ra = 10^4. It can be seen that the flow field is almost identical as Fig. 3.24. As seen

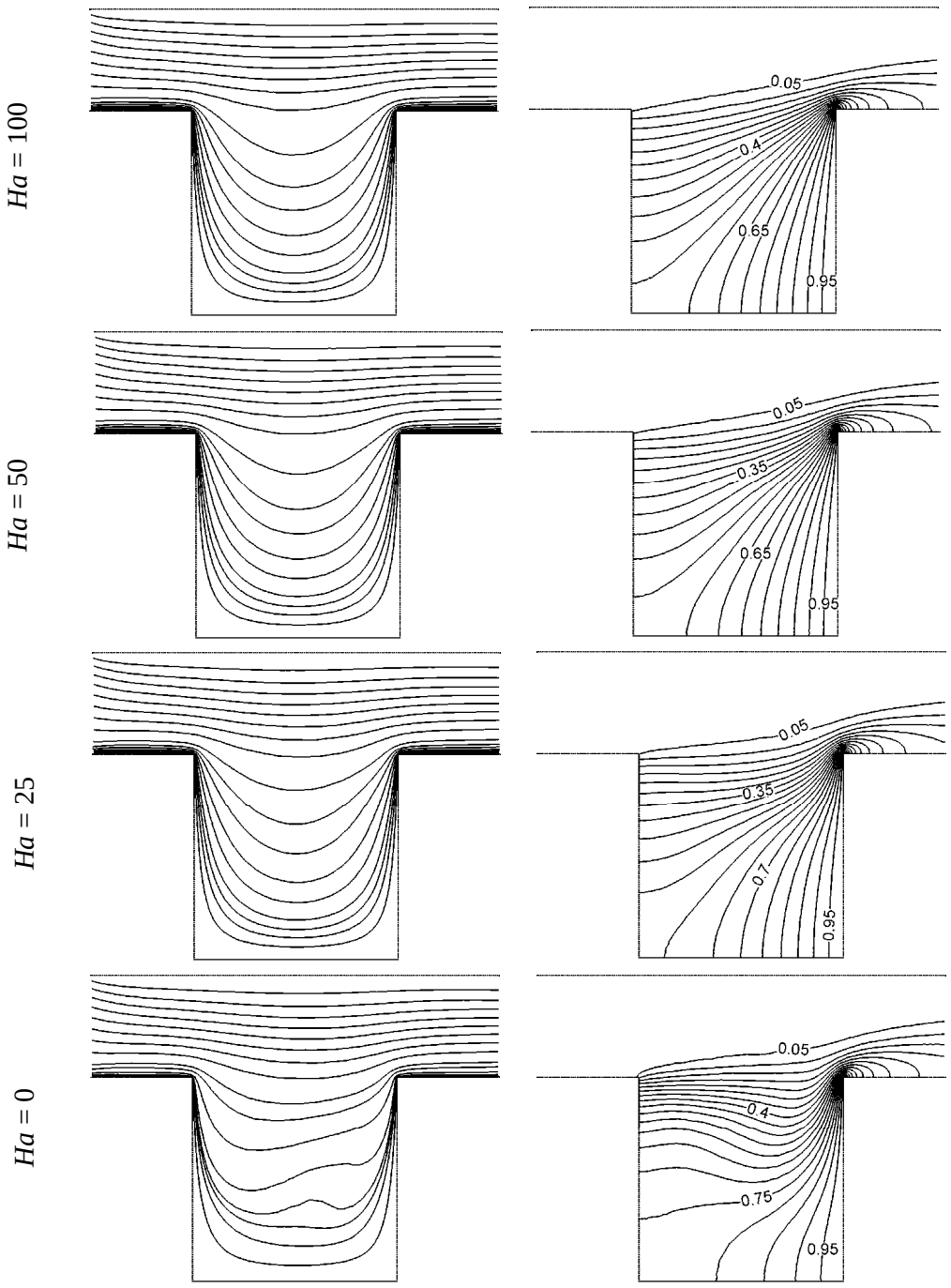

Fig. 3.21 (a) Streamlines and (b) Isotherms for case 3 at $Ra = 10^3$, $AR = 1$ and selected values of Hartmann number Ha.

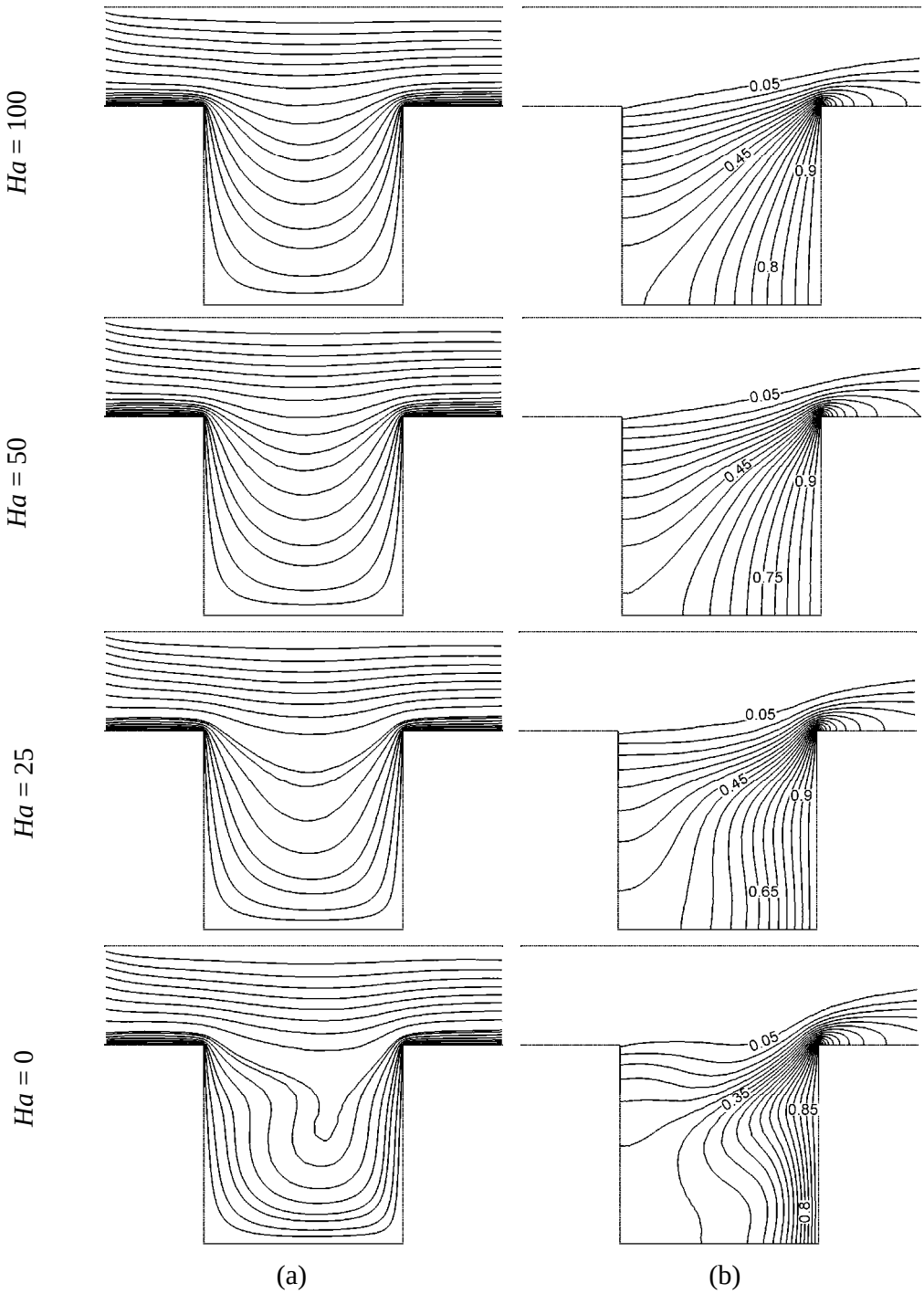

Fig. 3.22 (a) Streamlines and (b) Isotherms for case 3 at $Ra = 10^4$, $AR = 1$ and selected values of Hartmann number Ha.

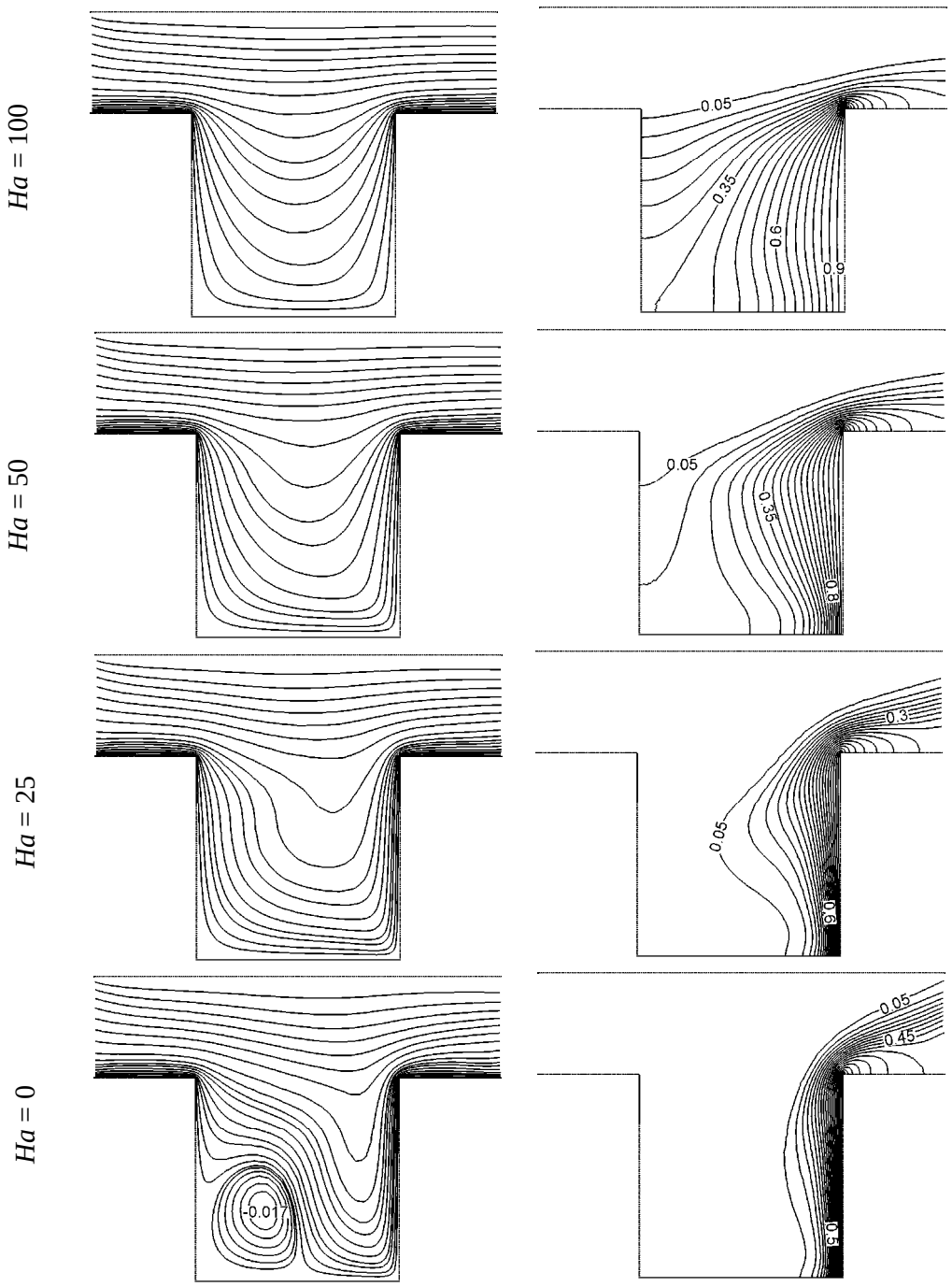

Fig. 3.23 (a) Streamlines and (b) Isotherms for case 3 at $Ra = 10^5$, $AR = 1$ and selected values of Hartmann number Ha.

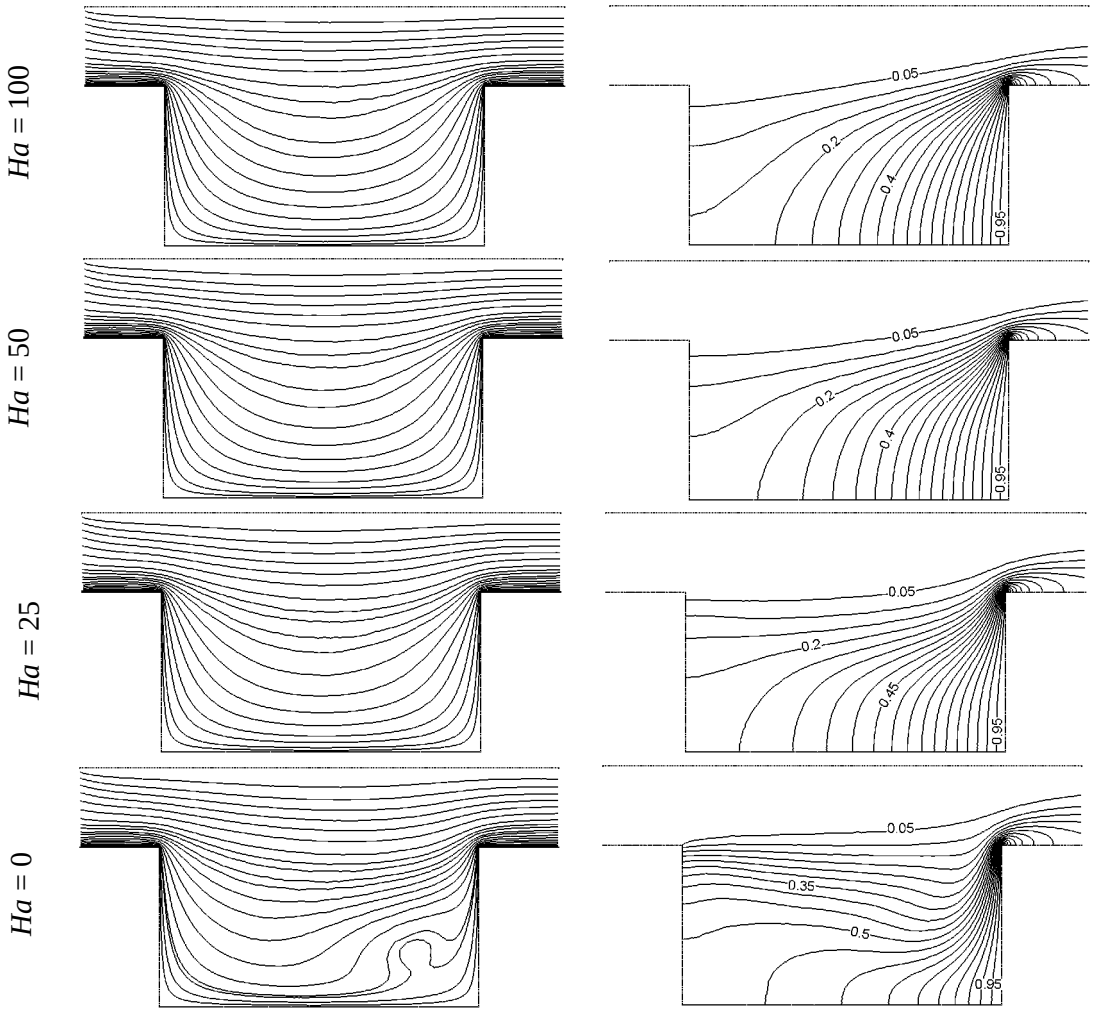

Fig. 3.24 (a) Streamlines and (b) Isotherms for case 3 at $Ra = 10^3$, AR = 2 and selected values of Hartmann number *Ha*.

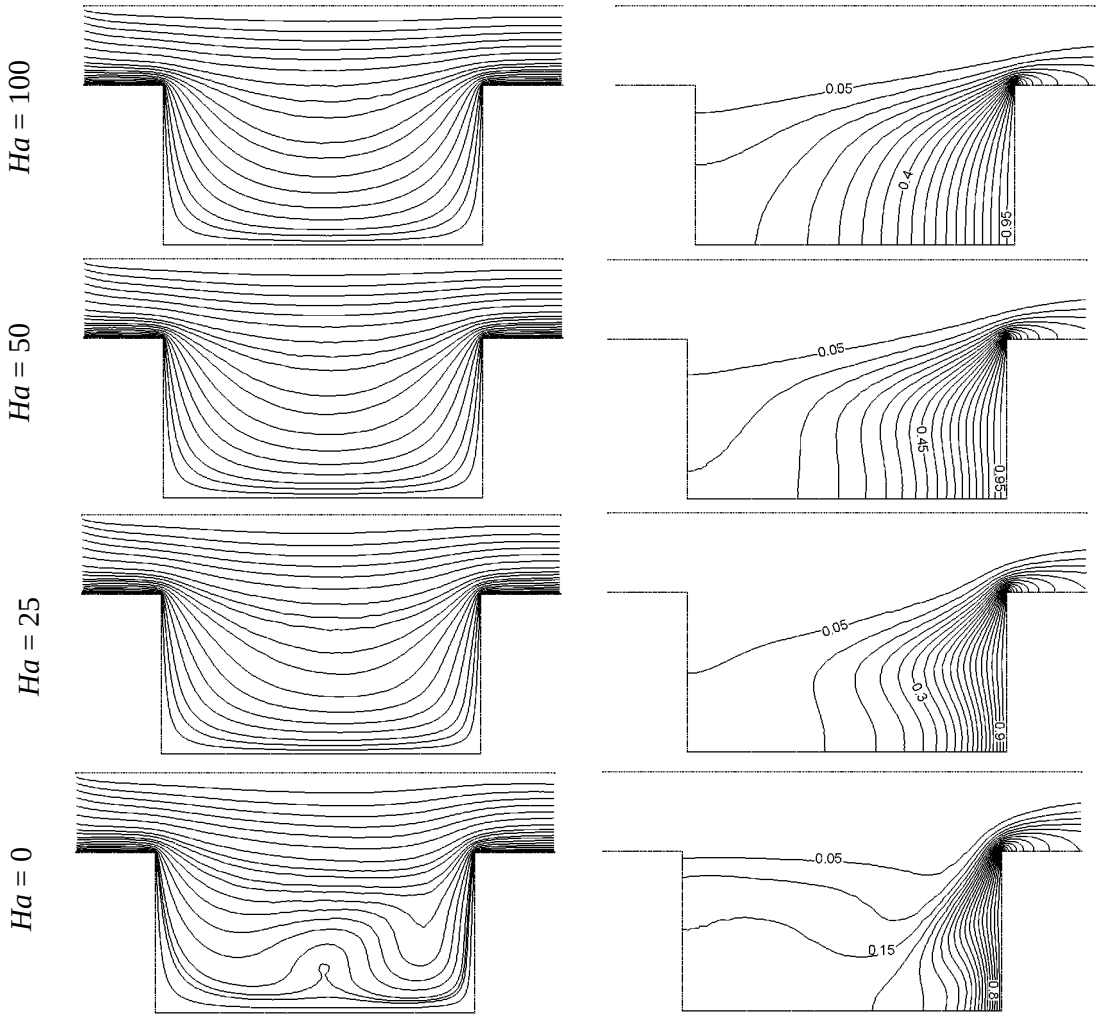

Fig. 3.25 (a) Streamlines and (b) Isotherms for case 3 at $Ra = 10^4$, $AR = 2$ and selected values of Hartmann number Ha.

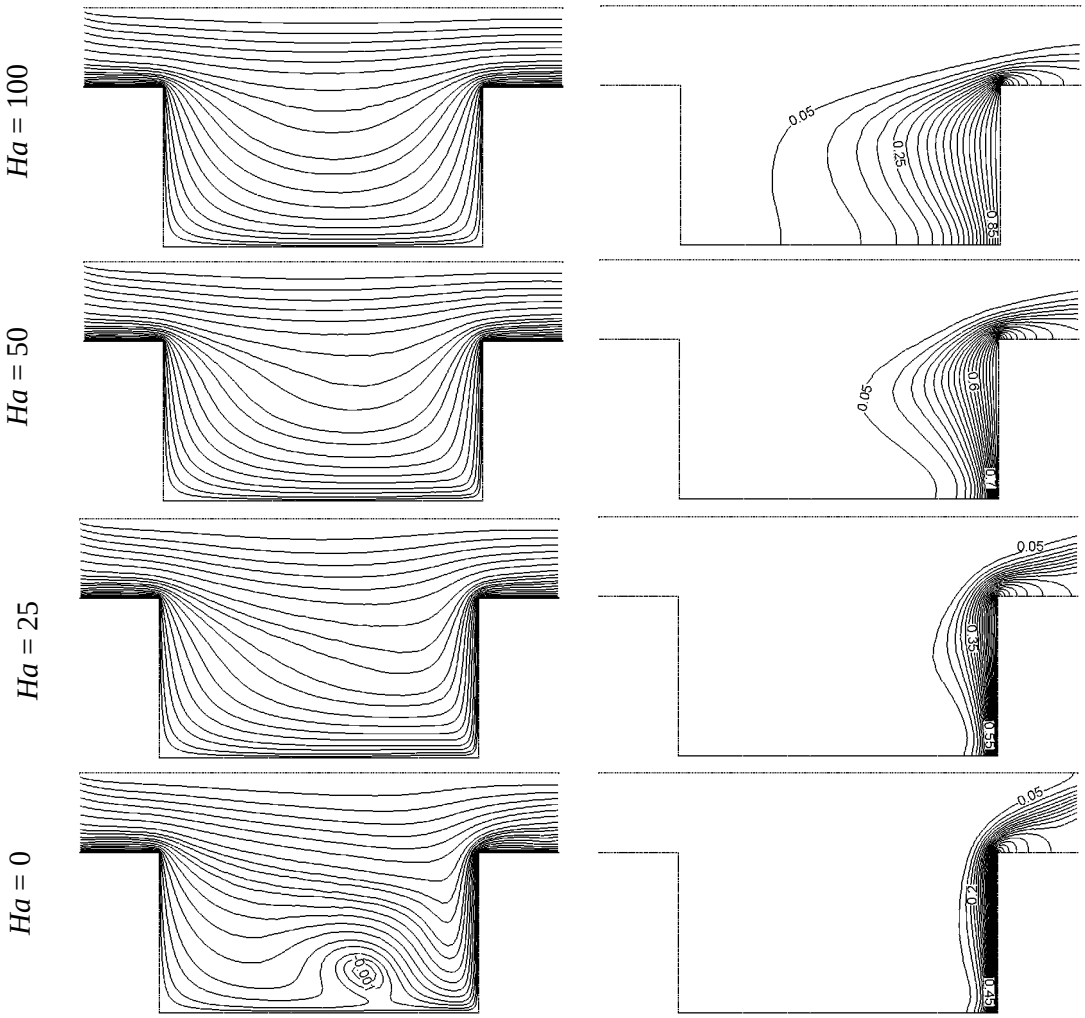

Fig. 3.26 (a) Streamlines and (b) Isotherms for case 3 at $Ra = 10^5$, $AR = 2$ and selected values of Hartmann number Ha.

from the right column of Fig. 3.25, thermal boundary layer becomes thicker with decreasing of Hartmann number. For Ha = 50 and 100, higher values isotherms are parallel to the heated wall. However, this parallel distribution is distorted for lower values of Hartmann number. The distortion of isothermal lines appears due to the high convective current inside the cavity. Distortions of isothermal lines start to disappear with increasing Hartmann number.

The effect of Hartmann number on the flow field and temperature fields has been revealed in Fig 3.26 at Ra = 10^5 and AR = 2. One may notice that the flow fields are almost alike as Figs. 3.24 – 3.25 for higher values Hartmann number Ha (= 25, 50 and 100). But, an interesting result is found that a very small circulating cell is formed in absence of magnetic field. As seen from the left column of this figure, an amount of fluid near the heating wall of the cavity is activated so as to create a buoyancy-induced clockwise rotating cell for the lowest value of *Ha* = 0. On the other hand, the thermal layer becomes thicker with decreasing of Hartmann number. In addition, it is observed that the higher values isotherms are more tightened at the vicinity of the heated wall of the cavity. As Hartmann number increases, isothermal lines inside the cavity approaches more and more towards the conduction-like distribution pattern of isothermal lines. For large Hartmann number *Ha* = 50 and 100, the convection is almost suppressed, and the isotherms are almost parallel to the horizontal wall, indicating that a quasiconduction regime is reached. However, in the remaining area near the right wall of the cavity, the temperature gradients are very small.

Fig. 3.27 (a) and (b) illustrate the average Nusselt number and average fluid temperature at the exit port, respectively while AR = 1. The figures are given for different Rayleigh numbers at preferred values of Hartmann numbers. Both Nusselt number and average fluid temperature at the exit port show similar trends. In addition, it is clearly noticed that both heat transfer and average fluid temperature are decreased with increasing of Hartmann numbers. Pressure and temperature gradient in the domain for different Rayleigh number while AR = 1 is offered in Fig. 3.28. It is found that pressure is positive for lower values of Ra (= 10^3 and 10^4) at selected values of Hartmann numbers. On the contrary, for higher value of Ra (= 10^5), pressure is decreasing also it starts to take negative value for Ha $\geq$ 38. However,

(a)

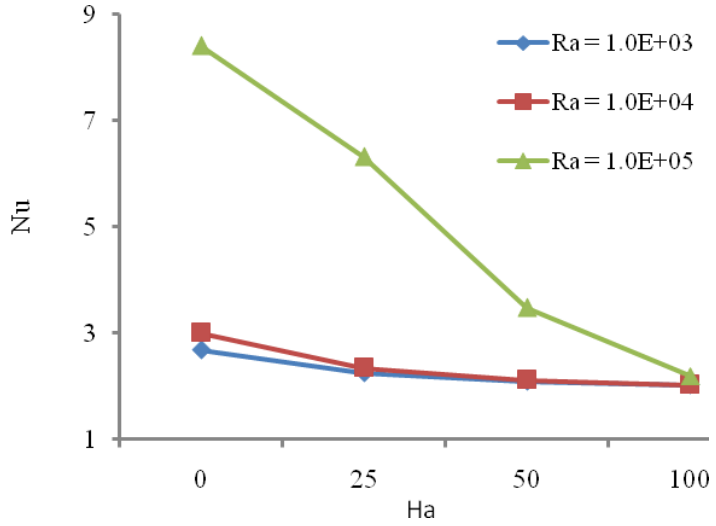

(b)

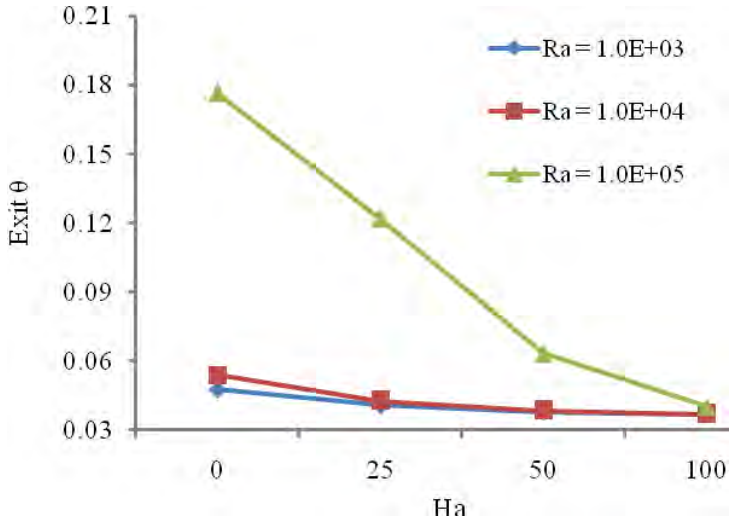

Fig. 3.27 (a) Average Nusselt number and (b) average fluid temperature at the exit port versus Hartmann number *Ha* for the case 3 at *AR* = 1 and selected values of Rayleigh number *Ra*.

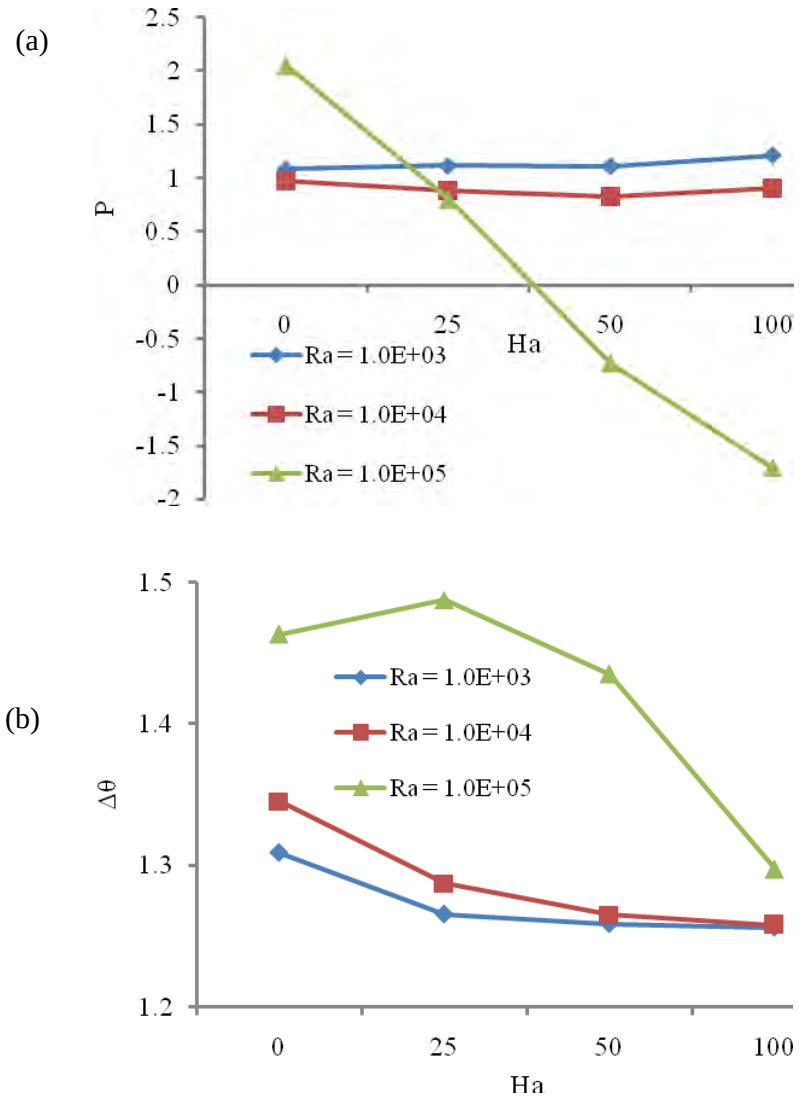

Fig. 3.28 (a) Pressure and (b) temperature gradient in the domain versus Hartmann number *Ha* for the case 3, at *AR* = 1 and selected values of Rayleigh number *Ra*.

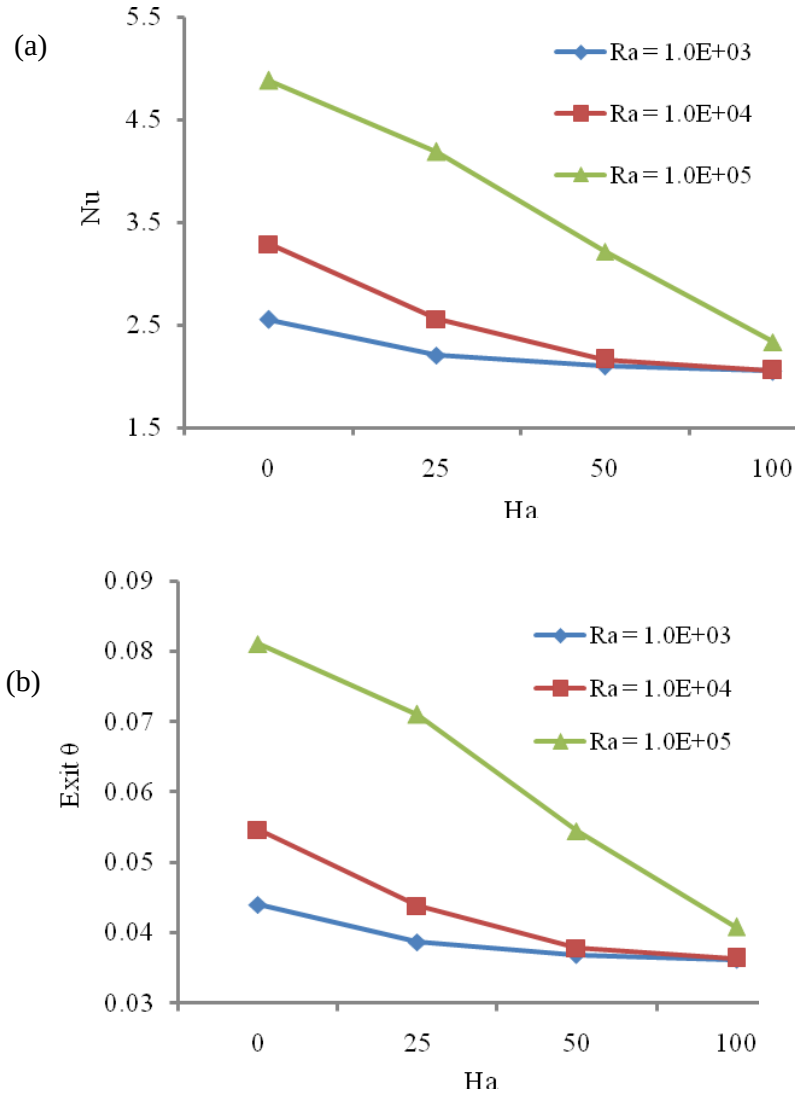

Fig. 3.29 (a) Average Nusselt number and (b) average fluid temperature at the exit port versus Hartmann number *Ha* for the case 3 at *AR* = 2 and selected values of Rayleigh number *Ra*.

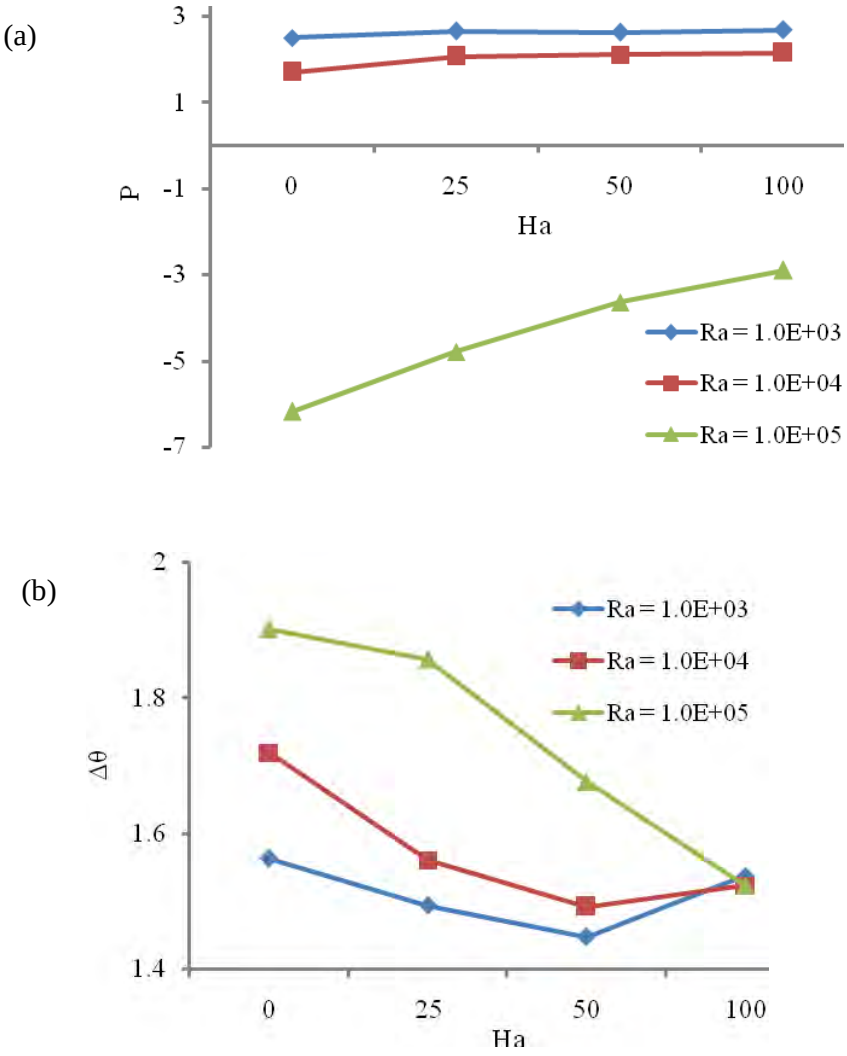

Fig. 3.30 (a) Pressure and (b) temperature gradient in the domain versus Hartmann number *Ha* for the case 3, at *AR* = 2 and selected values of Rayleigh number *Ra*.

temperature gradient is shown in Fig. 3.28 (b). As seen from the figure, broad sight of temperature gradient show decreasing behavior with Rayleigh number.

Variation of average Nusselt number and average fluid temperature at the exit port have been presented in Fig. 3.29 (a) and (b), respectively while AR = 2. It can easily be seen that both of the average Nusselt number and fluid temperature at the exit port gives alike trends. Furthermore, both heat transfer rate and average fluid temperature are decreased with rising of Hartmann numbers. It is also noticed that the heat transfer rate decreases straightly for Ra = 10^5 with increasing of magnetic force.

On the other hand, pressure and temperature gradient in the domain for different Rayleigh number while AR = 2 is presented in Fig. 3.30. It is seen that pressure is positive up to Ra = 10^4. But negative values are produced for increasing of Rayleigh number. Additionally, pressure is falling with decreasing Ha for Ra = 10^5. Also, temperature gradient is shown in Fig. 3.30(b). It is clearly seen from the figure, temperature gradient is decreasing for Ra = 10^5 with rising values of Hartmann numbers. But, the temperature gradient is declining for Ra (= 10^3 and 10^4) up to Ha =50 later on it is increasing.

CHAPTER 4

CONCLUSIONS

Mixed convection in a channel with a cavity heated from different sides under the influence of the applied magnetic force has been investigated numerically. The results are presented for flow and thermal fields as well as heat transfer for the channel with an enclosure subjected to constant hot temperature at a wall of the cavity while the remaining sidewalls are kept adiabatic. Finite element method is used to solve governing equations. Comparisons with the beforehand published work are performed and found to be in excellent agreement. The influences of Rayleigh number, the Hartmann number and the cavity aspect ratio have been reported. The various ideas and results have been discussed in detail at the relevant chapters of the thesis. In the present chapter an attempt is made to summarize the concepts presented and results obtained in the work reported already. A section on the scope of further work on associated fields of investigation is also included.

4.1 SUMMARY OF THE MAJOR OUTCOMES

Three different cases were considered based on heater position in the cavity as the left vertical side (Case 1), bottom side (Case 2) and right vertical side (Case 3). Prandtl number is chosen as Pr = 7.1 and Reynolds number is fixed at Re = 100.

The following main concluding remarks are drawn from the present study:

(i) Flow strength and heat transfer increase with Rayleigh number for all cases.

(ii) Flow velocity is reduced with increasing of Hartmann number, and this reduces flow strength and heat transfer. Thus, magnetic field can be a control parameter for heat transfer and fluid flow in open ended channel flow with cavity.

(iii) Each case is showed different behavior on the temperature distribution and flow field. Higher temperature gradient is observed in Case 3 when the heater locates on to the right wall.

(iv) Heat transfer is increased with increasing of Rayleigh number and higher fluid temperature is formed for the highest value of Rayleigh number in Case 3.

(v) Highest mean Nusselt number is formed for Ra = 10^5 in Case 3. For lower values of Rayleigh number, changing of location of the heater becomes insignificant.

(vi) Conduction mode of heat transfer becomes dominant for low values for Case 1.

(vii) Pressure inside the domain becomes almost zero for lower values of Rayleigh numbers and pressure becomes negative at the highest value of Rayleigh number.

(viii) The influence of cavity aspect ratio on fluid flow and temperature field is found to be pronounced. The heat transfer rate for lower cavity aspect ratio is higher than for higher aspect ratio.

4.2 FURTHER WORKS

The following can be put forward for the further works as follow-ups of the present research as.

- Double diffusive mixed convection can be analyzed through including the governing equation of concentration conservation.
- Investigation can be performed by using magnetic fluid instead of electrically conducting fluid within the porous medium and changing the boundary conditions of the cavity's walls.
- The study can be extended for turbulent flow using different fluids, different thermal boundary conditions such as constant heat flux or radiation and unsteady flow.
- Only two-dimensional fluid flow and heat transfer has been analyzed in this thesis. So this deliberation may be extended to three-dimensional analyses to investigate the effects of parameters on flow fields and heat transfer in cavities.

REFERENCES

Angirasa, D., “Mixed convection in a vented enclosure with isothermal vertical surface”, Fluid Dyn. Res. Vol. 26, pp. 219-233, 2000.

Aminossadati, S. M., and Ghasemib, B., “A numerical study of mixed convection in a horizontal channel with a discrete heat source in an open cavity”, European J. Mechanics B/Fluids, Vol. 28, pp. 590-598, 2009.

Bhuvaneswari, M., Sivasankaran, S., and Kim, Y.J., Magnetoconvection in a square enclosure with sinusoidal temperature distributions on both side walls, Numer. Heat Transfer A, Vol. 59(3), pp 167-184, 2011.

Chamkha, A. J., “Hydromagnetic combined convection flow in a vertical lid-driven cavity with internal heat generation or absorption”, Numer. Heat Transfer, Part A, Vol. 41, pp. 529-546, 2002.

Gau, C., Jeng, Y.C., and Liu, C.G., “An experimental study on mixed convection in a horizontal rectangular channel heated from a side”, ASME J. Heat Transfer, Vol. 122, pp. 701–707, 2000.

Hsu, T.H., and Wang, S. G., “Mixed convection in a rectangular enclosure with discrete heat sources”, Numer. Heat Transfer, Part A, Vol. 38, pp. 627-652, 2000.

Khanafer, K., Vafai, K., and Lightstone, M., “Mixed convection heat transfer in two-dimensional open-ended enclosure”, Int. J. of Heat and Mass Transfer, Vol. 45, pp. 5171-5190, 2002.

Leong, J.C., Brown, N.M., and Lai, F.C., Mixed convection from an open cavity in a horizontal channel, Int. Commun. Heat Mass Transfer Vol. 32, pp 583-592, 2005.

Mahmud, S., Tasnim, S. H., and Mamun, M. A. H., “Thermodynamic analysis of mixed convection in a channel with transverse hydromagnetic effect”, Int. J. of Thermal Sciences, Vol. 42, pp. 731-740, 2003.

Manca, O., Nardini, S., Khanafer, K., and Vafai, K., “Effect of heated wall position on mixed convection in a channel with an open cavity”, Numer. Heat Transfer, Part A, Vol. 43, pp. 259–282, 2003.

Manca, O., Nardini, S., and Vafai, K., “Experimental investigation mixed convection in a channel with an open cavity”, Experimental Heat Transfer, Vol. 19, pp. 53–68, 2006.

Omri, A., and Nasrallah, S. B., “Control volume finite element numerical simulation of mixed convection in an air-cooled cavity”, Numer. Heat Transfer, Part A, Vol. 36, pp. 615–637, 1999.

Ogot, E.B., Magnetohydrodynamic natural convection flow in an enclosure with a finite length heater using the differential quadrature (DQ) method, Numer. Heat Transfer A, Vol. 58(11), pp 900-921, 2010.

Oztop H.F., Influence of exit opening location on mixed convection in a channel with volumetric heat sources, Int. Comm. Heat Mass Transfer, Vol. 37, pp 410-415, 2011.

Oztop, H.F., Oztop, M., Varol, Y., Numerical simulation of Magnetohydrodynamic buoyancy-induced flow in a non-isothermally heated square enclosure, Commun. Nonlinear Sci. and Numer. Simulations, Vol. 14, pp 770-778, 2009.

Papanicolaou, E., and Jaluria, Y., "Mixed convection from an isolated heat source in a rectangular enclosure", Numer. Heat Transfer, Part A, Vol. 18, pp. 427–461, 1990.

Papanicolaou, E., and Jaluria, Y., "Transition to a periodic regime in mixed convection in a square cavity", J. Fluid Mech., Vol. 239, pp. 489–509, 1992.

Papanicolaou, E., and Jaluria, Y., "Mixed convection from a localized heat source in a cavity with conducting walls: A numerical study", Numer. Heat Transfer, Part A, Vol. 23, pp. 463–484, 1993.

Papanicolaou, E., and Jaluria, Y., "Mixed convection from simulated electronic components at varying relative positions in a cavity", J. Heat Transfer, Vol. 116, pp. 960–970, 1994.

Piazza, I.D., and Ciofalo, M., MHD free convection in a liquid-metal filled cobic enclosure I. Differential heating, Int. J. Heat Mass Transfer, Vol. 45, pp 1477–1492, 2002.

Rahman, M. M., Alim, M. A., Mamun, M. A. H., Chowdhury, M.K. and Islam, A.K.M.S., "Numerical Study of Opposing Mixed Convection in a Vented Enclosure", ARPN J. of Engineering and Applied Sciences, Vol. 2, No. 2, pp 25-36, 2007.

Rahman, M. M., Alim, M. A., and Chowdhury, M. K., Magnetohydrodynamic mixed convection around a heat conducting horizontal circular cylinder in a rectangular lid-driven cavity with joule heating", J. Sci. Res. Vol. 1(3), pp 461-472, 2009.

Raji, A., and Hasnaoui, M., "Mixed convection heat transfer in a rectangular cavity ventilated and heated from the side", Numer. Heat Transfer, Part A, Vol. 33, pp. 533–548, 1998a.

Raji, A., and Hasnaoui, M., "Correlations on mixed convection in ventilated cavities". Revue Ge´ne´rale de Thermique, Vol. 37, pp. 874–884, 1998b.

Raji, A., and Hasnaoui, M., “Mixed convection heat transfer in ventilated cavities with opposing and assisting flows”, Int. J. Computer-Aided Eng. Software, Vol. 17(5), pp. 556–572, 2000.

Rahman, M.M., Saidur, R, Rahim, N.A., “Conjugated effect of joule heating and magneto-hydrodynamic on double-diffusive mixed convection in a horizontal channel with an open cavity”, Int. J. Heat Mass Transfer, Vol. 54, pp 3201-3213, 2011a.

Rahman, M.M, Parvin, S, Saidur R, and Rahim, N.A., “Magnetohydrodynamic mixed convection in a horizontal channel with an open cavity”, Int. Comm. Heat Mass Transfer, Vol. 38, pp 184-193, 2011b.

Saeidi, S. M., and Khodadadi, J. M., “Forced convection in a square cavity with inlet and outlet ports”, Int. J. of Heat and Mass Transfer, Vol. 49, pp. 1896-1906, 2006.

Sahoo, D., and Sharif, M. A. R., “Mixed-convective cooling of an isothermal hot surface by confined slot jet impingement”, Numer. Heat Transfer, Part A, Vol. 45, pp. 887-909, 2004.

Sarris, I. E., Kakarantzas, S. C., Grecos, A. P., and Vlachos, N. S., “MHD natural convection in a laterally and volumetrically heated square cavity”, Int. J. of Heat and Mass Transfer, Vol. 48, pp. 3443-3453, 2005.

Singh, S., and Sharif, M. A. R., “Mixed convective cooling of a rectangular cavity with inlet and exit openings on differentially heated side walls”, Numer. Heat Transfer, Part A Vol. 44, pp. 233–253, 2003.

Sposito, G., and Ciofalo, M., Fully developed mixed Magnetohydrodynamic convection in a vertical square duct, Numer. Heat Transfer A, Vol. 53(9), pp 907-924 2008.

Wang, Q., and Jaluria, Y., “Instability and heat transfer in mixed convection flow in a horizontal duct with discrete heat sources”, Numer. Heat Transfer, Part A, Vol. 42, pp. 445-463, 2002.

Xu, B., Li, B.Q., Stock, D.E., An experimental study of thermally induced convection of molten gallium in magnetic fields, Int. J. Heat Mass Transfer 49 (2006) 2009–2019.

Zienkiewicz, O. C. and Taylor, R. L., “The finite element method”, Fourth Ed., McGraw-Hill, 1991.